Koninklijk Meteorologisch Instituut van België

Institut Royal Météorologique de Belgique

Royal Meteorological Institute of Belgium

RMI

Quantitative Precipitation Forecasts based on radar observations: principles, algorithms and operational systems

dr. Maarten Reyniers

2008

Quantitative Precipitation Forecasts
based on radar observations:
principles, algorithms and operational systems
dr. Maarten Reyniers

Scientific committee:
dr. ir. Steven Dewitte
dr. ir. David Dehenauw
dr. ir. Laurent Delobbe
dr. Alex Deckmyn

Contents

CONTENTS

1   Introduction

Amongst all meteorological phenomena, precipitation has one of the largest impacts on the human society. It affects not only our daily lives, it has also a large impact on (urban and rural) hydrology, agriculture, water supply, industrial activities etc. Moreover, severe precipitation events can lead to human, economical and ecological disasters with huge economical consequences.

The forecast of precipitation is, however, a most challenging task. Since it is governed by complex microphysical processes, the exact circumstances for a cloud to form precipitation are still not fully understood. But also on a macro-scale, the formation of precipitation is linked to very complex dynamical processes of the atmosphere. Moreover, precipitation can be a very local phenomenon, e.g. in the case of an isolated convective event, acting on scales much smaller than the mesoscale, and sometimes even smaller than the grid scale of the most recent NWP models (note that also very large widespread precipitation structures exist, e.g. in the case of the slow passage of a cold front). Due to these incompatible scales of precipitating structures and (most) NWP models, the capabilities of the existing NWP models in the prediction of precipitation at a specific location are rather limited. Moreover, an incomplete data assimilation in the stage of the initialisation of an NWP model can lead to unreliable precipitation predictions for short lead times of 0-6 h. In other words, an incomplete assimilation in an NWP model limits the skill of NWP precipitation forecasts for short lead times considerably, since the model does not cover adequately enough the present situation.

The abovementioned shortcomings of NWP models indicate that Quantitative Precipitation Forecasts (QPFs) for short lead-times clearly require a different strategy. Radar observations provide precipitation maps with high spatial (typically $\sim$1 km) and temporal ($\sim$5 min) resolution, and are therefore ideally suited to act as the basic building blocks of operational precipitation nowcasts. The basic idea for a radar based QPF is the spatio-temporal extrapolation of the precipitating areas. A number of strategies for this extrapolation are elaborated in the literature, but most of them can be traced back to some basic concepts or principles. These principles will be discussed in Sect. 2. In Sect. 3, we give a concise overview of the existing QPF algorithms based on these principles. In Sect. 4, we review the QPF systems currently operational in meteorological services worldwide, together with some recent systems that are developed for research without being operational. These systems are usually blends of the algorithms described in Sect. 3 and other sources of data (e.g. NWP) and/or techniques. In some cases, however, the distinction between a QPF "algorithm" and a QPF "system" is hard to make, and clearly some overlap exists between Sect. 3 and Sect. 4. In Sect. 5, we will formulate the prerequisites for a future operational nowcasting system at the RMI, and discuss the requirements of such a system for the potential internal and external users. We end with the main conclusions (Sect. 6). At the end of this paper (p. 50), a list of acronyms is provided, together with a short note on verification statistics.

The variety of QPF systems currently available is very large. Nevertheless, two different strategies prevail in this jungle of systems: systems based on *cell tracking* and systems based on *area tracking*. The former strategy treats precipitating cells as individual entities, and concentrates on the development and displacement of these entities to make a prediction of the future situation. In the latter strategy, area tracking, a rainrate image is divided in a grid of boxes, and for each box, a corresponding box is searched in the next image. In such way, a velocity field can be constructed that is used to predict the future situation. Cell tracking systems are principally designed to locate severe weather objects (mostly convective) and to give qualitative severe weather warnings. This is a different goal then using the gridded fields of area trackers. On the other hand, cell tracking systems are generally not designed (and thus not useful) for stratiform precipitation. Area trackers are clearly superior in this task. Therefore, the

performance of a system should always be tested in situations for which it is designed for. Another consequence is that two different QPF systems cannot be compared if they are designed for different purposes. The reader should keep this in mind while reading this document.

Radar observations are subject to several errors and uncertainties themselves. It is beyond the scope of this paper to discuss these uncertainties, since they are discussed in numerous other works. We refer the reader to two standard text books for this matter, being Rinehart (2004) for an introduction in the basic principles, and Doviak and Zrnić (1993) for an in-depth reading on radar meteorology. Nevertheless, quality control of radar observations is a very important issue, since poor quality can destroy any sophisticated QPF algorithm.

It is also not in the scope of this paper to discuss the current status of the operational radars in Belgium. Here, we only remind that there are two C-band Doppler weather radars in Belgium. One is operated by our own institute, and is located in Wideumont, in the province of Luxembourg in the south of the country (Fig. 1, see e.g. Berne et al., 2005; Delobbe and Holleman, 2006, for more technical details of this radar). The other one is the property of Belgocontrol, the public company in charge of the safety of civil air traffic in Belgium. This radar is located in Zaventem, near the airport of Brussels. Radar data are exchanged in real time between the company and our institute. In the text, the term *Belgian composite* (Fig. 2) refers to the composite of the pseudo-CAPPI images (1500 m) of these two radars. A pseudo-CAPPI image represents a horizontal cross-section of radar data at constant altitude, complemented by the highest elevation beam for the shortest distances, and the lowest beam for the longest distances. Apart from the radar in Zaventem, the RMI also receives images from the radar in Avesnois (Fr), which is property of Météo France, and images from the radar in Neuheilenbach (D), which is property of the Deutscher Wetterdienst (DWD). The four radars are also integrated in OPERA, the European radar network supported by EUMETNET (see e.g. Holleman et al., 2008, for the current status of this project).

We end this introduction with some remarks about the terminology used in this paper. During a *scan* the antenna of a radar performs at a few elevations a full turn around its vertical axis. The elevations are defined by the *scan strategy*. A complete scan produces a *volume file*, also referred to as a 3D radar image. A number of 2D images can be derived from this volume file, like (pseudo-)CAPPI, MAX (maximum values in vertical direction), VIL (Vertically Integrated Liquid), hail probability, accumulation maps, etc...The term *rainrate image* or *rainrate field* refers to such a (pseudo-)CAPPI 2D image, on which the reflectivity (Z) is transformed to rainrate (R), using some kind of Z-R relation. Note that many of the equations in the paper are applicable to both quantities. In such cases, we will use the symbol R.

Figure 1: The C-band Doppler radar located in Wideumont, in the south of Belgium. The radar is operated by the our institute, and was installed in 2001. More information on its operation can be found in Delobbe and Holleman (2006).

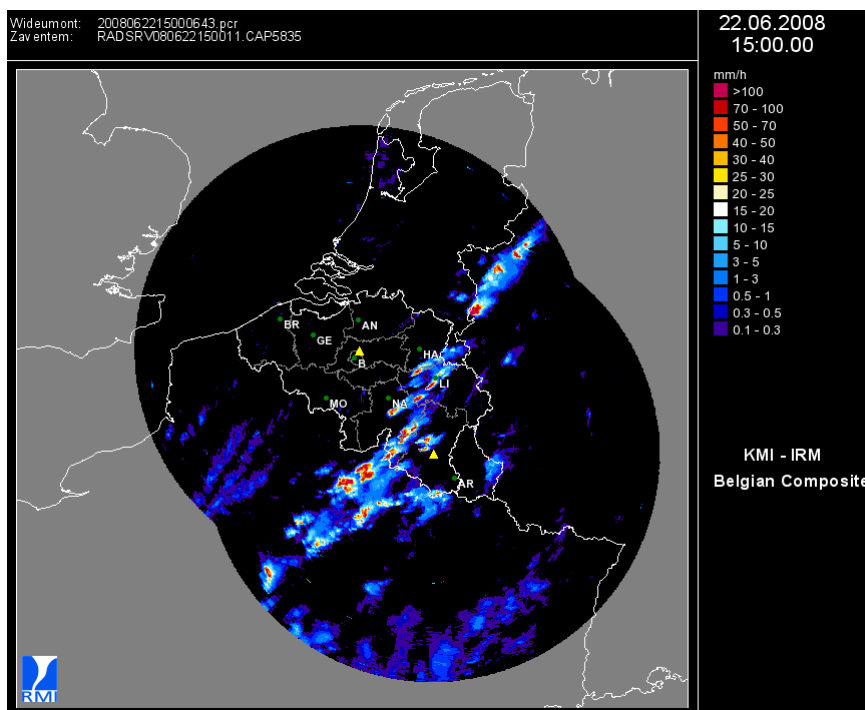Figure 2: The term *Belgian composite* refers the combination of the pseudo-CAPPI images of the radar of Zaventem (operated by Belgocontrol) and the one of Wideumont (operated by the RMI). A pseudo-CAPPI image represents a horizontal cross-section of radar data at constant altitude (here 1500 m), complemented by the highest elevation beam for the shortest distance to the radar, and the lowest beam for the longest distances.

2   QPF principles

2.1   Lagrangian persistence

Definitely the simplest QPF, but also the most perishable, is if the current radar image is taken as the prediction. This type of forecast is dubbed **Eulerian persistence** and is usually only taken as a reference forecast: the skill of a specific forecast is often compared with Eulerian persistence. A forecast in which the precipitation field is advected by a velocity field (vector field), leaving the total intensity unchanged, is called **Lagrangian persistence**:

$$\frac{dR}{dt} \equiv 0 \tag{1}$$

with $R(x, y)$ the rainrate at point $\mathbf{x}(x, y)$. In this equation, dR/dt is seen in the coordinates of the flowing data (Lagrangian framework). Eq. (1) can be further written in the rigid (image) coordinates as

$$\frac{\partial R}{\partial x}\frac{\partial x}{\partial t} + \frac{\partial R}{\partial y}\frac{\partial y}{\partial t} + \frac{\partial R}{\partial t} = 0$$

or

$$u\frac{\partial R}{\partial x} + v\frac{\partial R}{\partial y} + \frac{\partial R}{\partial t} = 0 \tag{2}$$

$$\mathbf{v} \cdot \nabla R + \dot{R} = 0$$

with $\mathbf{v} = (u, v)$ the velocity field. In this equation, the rainrate field R is known from the radar scan, and the velocity field $\mathbf{v}$ has to be determined. Often the reflectivity Z is advected instead of the rainrate (derived from the reflectivity). In computer science, Eq. (2) is often referred to as the *optical flow* (OF) equation, or simply *optical flow*. Optical flow is defined as the determination of apparent movement by the analysis of subsequent (discrete) observations. In practice, the OF equation has a discrete nature

$$U\frac{\Delta R_n}{\Delta x} + V\frac{\Delta R_n}{\Delta y} + \frac{\Delta R_n}{\Delta t} = 0 \tag{3}$$

with R_n the rainrate at time n, and U, V the velocity components of the rainrate field (or reflectivity field if Z is used). The (discrete) spatial derivatives $\Delta R_n/\Delta x$ and $\Delta R_n/\Delta y$ are calculated from the current rainrate image R_n, while $\Delta R_n/\Delta t$ is derived from the difference between R_n and R_{n-1}.

The optical flow equation (Eq. 2) does not contain enough information to solve for the velocity field $\mathbf{v}$. Indeed, Eq. (2) contains two unknowns u and v. QPF schemes using optical flow usually invoke an additional minimisation, like e.g. a minimisation of a cost function C in the neighbourhood Ω of type

$$C = \sum_{\Omega} w \cdot (\mathbf{v} \cdot \nabla R + \dot{R})^2$$

where weight w can be a function of image coordinates and/or neighbourhood coordinates. This minimisation leads to an overdetermined system from which the "best" u and v estimates are derived (Peura and Hohti, 2004). Alternatives for the additional equation(s) to provide sufficient information to solve for $\mathbf{v}$ are

• the minimisation of $\nabla^2\mathbf{v}$ as applied in a version of GANDOLF (see Sect. 4; Bowler et al., 2004b). This is equivalent to minimising

$$\frac{\partial^2 u}{\partial x^2} + \frac{\partial^2 u}{\partial y^2} \quad \text{and} \quad \frac{\partial^2 v}{\partial x^2} + \frac{\partial^2 v}{\partial y^2}$$

which forces the flow to be smooth (*smoothness constraint*);

• the minimisation of

$$\frac{\partial u}{\partial x} + \frac{\partial v}{\partial y}$$

as used in the COTREC scheme (see Sect.3.2; Li et al., 1995).

The additional equations that are added to the OF equation, are called the *Optical Flow Constraint* (OFC) in the literature. Confusingly enough, in some papers Eq. (2) is regarded as the OFC, while the additional equations then act as the OF equation.

Eq. (3) can be extended with a source-sink term, which can take the form

$$U\frac{\Delta R_n}{\Delta x} + V\frac{\Delta R_n}{\Delta y} + \frac{\Delta R_n}{\Delta t} = f(Z_n, Z_{n-1}, ..., Z_{n-k}, \mathbf{a}) + w$$

with f a function of the k previous rainrate or reflectivity fields and a list of m parameters $\mathbf{a} = (a_1, a_2, ..., a_m)$. w is a noise component. Such an approach clearly does not preserve the total rainrate, and hence Lagrangian persistence is no longer valid. Grecu and Krajewski (2000) tested a back-propagation neural network (BPNN) scheme to model function $f(\cdot)$, but concluded that there was only little benefit from such a complicated neural-network based procedure compared to the relatively simple Lagrangian advection. Of course, the specific setup presented in that study cannot account for all possible formulations of neural networks (and hence functions f), but the result suggests that more complex schemes do not always guarantee better QPFs than simpler schemes.

Although the construction of a velocity field $\mathbf{v}(u, v)$ through OF (Eq. (2) and an additional constraint) is mathematically well funded, it often leads to very noisy or erroneous velocity fields. Therefore, velocity fields are often deduced with other techniques. Two major techniques are frequently used in the QPF field, and are extensively described in the literature: *area tracking* methods and *cell* or *centroid tracking* methods.

2.2 Area tracking

Area tracking divides a rainrate image into a grid of boxes, and for each box, a corresponding box (in the sense of a maximum correlation) is searched in the next image. The collection of vectors realising the translation between the corresponding boxes, forms the velocity field $\mathbf{v}$. The procedure of an area tracker is illustrated in Fig. 3. This figure illustrates the concept of TREC (see Sect. 3.2; Rinehart and Garvey, 1978), but other correlation area trackers work very similar. The first image (*left panel* of Fig. 3) determines the spatial resolution for the displacement vectors. Around each grid point a tracking area is defined, called the box size. This box is compared to similar boxes within the searching range of the second image. The size of the searching range is defined by choosing a maximum velocity and the time lag between first and second image. For each pair of boxes of the first and second image the correlation coefficient is computed. The translation vector between a pair of boxes realising the maximum correlation coefficient is taken as a valid velocity vector. Unfortunately, the procedure as it is outlined above, leads to noisy velocity fields, often containing wrong vectors or divergent features. Several schemes are developed to smooth and/or correct these shortcomings. The basics of some of these schemes (e.g. COTREC; Li et al., 1995) are already explained above, in the context of OF. More details for some specific schemes are given in Sect. 3.2.

2.3 Cell tracking

In **Cell tracking** or **centroid tracking**, the evolution of *discrete objects* on consecutive radar images is followed. Every cell tracking algorithm has essentially two parts, a *detection algorithm* and a *matching algorithm*. In the first part, discrete objects (normally contiguous regions

RADAR SCAN TIME 1   RADAR SCAN TIME 2 (= TIME 1 + Δt)

RADAR ECHO

SPATIAL RESOLUTION OF   SEARCHING AREA   DISPLACEMENT   BEST FIT
DISPLACEMENT VECTORS   VECTOR   TIME 2
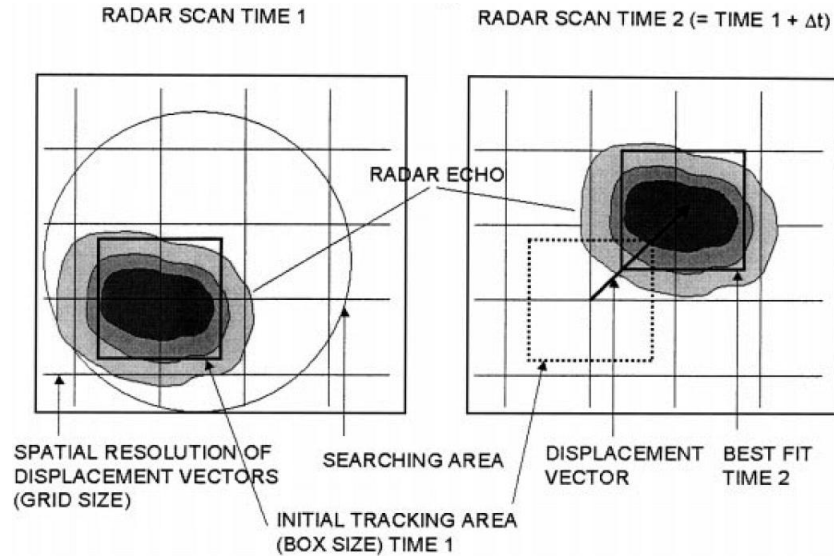(GRID SIZE)

INITIAL TRACKING AREA
(BOX SIZE) TIME 1

Figure 3: Concept of the TREC (Rinehart and Garvey, 1978) area tracking algorithm (see text for discussion). Other area trackers work very similar. Figure taken from Mecklenburg et al. (2000).

of high reflectivity, either in 2D images or in 3D volume scans) are identified on the scans, and their characteristics are stored in some kind of database structure. The characteristics are typically the centroid coordinates, the area, echo-tops, the (cell-based) VIL *(Vertically Integrated Liquid)*, etc... In the second part of the algorithm, the matching part, these characteristics are used to identify identical cells on consecutive images. Usually a searching area for cell identification is defined, based on previous cell velocities. The major advantage is that cell statistics can be derived from cell trackers, and statistical studies of precipitating cells become feasible. Moreover, intense convective cells exhibit often a dynamic behaviour that is very different from the larger enveloping rain area. Clearly, cell tracking is expected to perform better in convective situations. Several tracking algorithms are developed and discussed in the literature; we will discuss five of them in Sect. 3.1.

2.4   Spectral algorithms

Spectral algorithms provide an approach that relies on the observation that the smallest scales in a rainrate image are usually the least predictable, since their typical lifetimes are much shorter than the lifetimes of the larger structures. In a spectral algorithm, a reflectivity image of dimension $L \times L$ pixels is spatially decomposed into an additive cascade of n levels X_k, representing the kth scale of the decomposition, so that

$$dBZ_{i,j}(t) = \sum_{k=1}^{n} X_{k,i,j}(t), \quad i = 1, ..., L, \quad j = 1, ..., L \quad L = 2^n$$

with $dBZ_{i,j}$(t) the reflectivity in dB at pixel (i, j) at time t. Rainfall intensity R has a multiplicative structure, i.e. rainfields can be approximated by multiplying independent component processes at different scale (e.g. Veneziano et al., 1996). This multiplicative structure converts into a summation when taking the logarithm, and this is the reason why dBZ is taken for the decomposition, and not Z or R. X_k in the cascade represents the variability of the original field with structures of scales between $2^{-(k+1)}L$ and $2^{-k}L$ pixels. The decomposition as it is presented
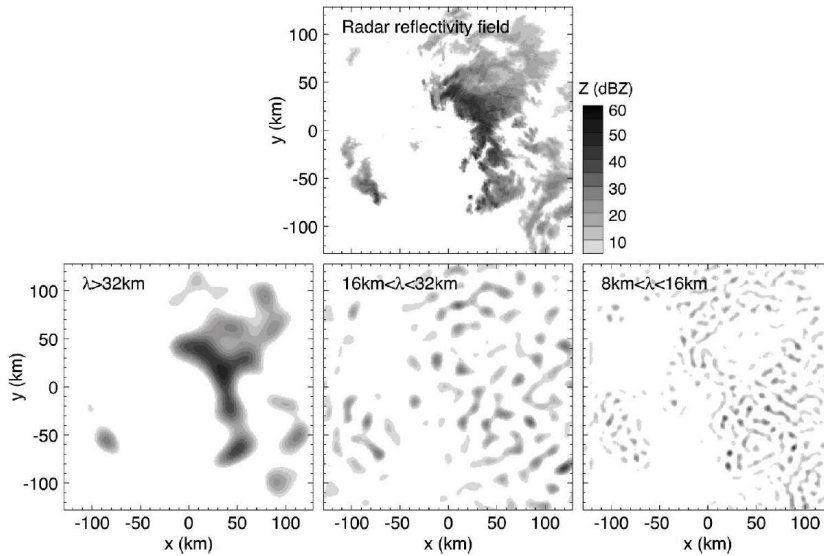
Figure 4: Illustration of the decomposition of a reflectivity field into a cascade of structures of different scales. The original reflectivity field is shown in the upper figure; three cascade levels are shown below: scales larger than 32 km (left), scales between 16 and 32 km (middle), and scales between 8 and 16 km. Figure taken from Berenguer et al. (2005).

here, is the method used in the S-PROG algorithm developed by Seed (2003). S-PROG is used in different nowcasting schemes (see Sect. 4). An example of a reflectivity field and the associated decomposition is given in Fig. 4. After the decomposition, the evolution of the levels is considered separately: a measure for the lifetime of a certain level is obtained by studying the correlation of that level at time t_1 and at time t_2 (= $t_1 + \Delta t$). A future rainrate image is then composed by the summation of the different levels, taking into account their predicted lifetime as weight. The levels with the larger structures will have high correlation values with previous levels, and thus these levels will dominate for large lead times.

On Fig. 4, one of the weaknesses of the method is readily seen: the presence of periodic structures in the smallest scales, that are clearly not present in the original reflectivity field. This is a well-known effect in spectral decompositions called the *Gibbs effect*. This Gibbs effect can be largely avoided by using local spectral decompositions, which can be realised using *wavelets*. Such a wavelet decomposition is implemented in the QPF system MAPLE, which is discussed in detail in Sect. 4.8.

Obviously, spectral algorithms do not provide an advection procedure on their own; the different levels of the cascade have to be advected by an additional procedure. Since the original set-up of S-PROG (Seed, 2003) was the study of the decomposition itself, the advection is done through a simple and robust area tracker applied to the original reflectivity field (and not to the different levels separately), producing only one displacement vector for the whole field. The advection is further refined in the recent nowcasting scheme STEPS (Bowler et al., 2006). An example of a nowcasting system using the spectral decomposition of S-PROG, but the advection scheme of the area tracker COTREC (Sect. 3.2) is given in Berenguer et al. (2005). Clearly spectral algorithms have left the research stage and are more and more integrated into operational nowcasting systems.

2.5   Expert systems

Expert systems is a generic name for nowcasting systems that combine one of the above-mentioned techniques with other data, conceptual models and/or explicit solutions of numerical equations. The main goal of these additions on top of the techniques presented above, is the ability to predict storm *initiation* or *decay*. Indeed, since the tracking algorithms are only based on reflectivity fields in the past, they are unable to predict any storm initiation. A variety of expert systems is developed in the last two decennia, ranging from relatively straightforward approaches as e.g. the TRT system in Switzerland (Hering et al., 2006), to the very complicated Auto-nowcaster (ANC; Mueller et al., 2003) of the National Center for Atmospheric Research (NCAR) in the U.S. Some of them (e.g. GANDOLF; Pierce et al., 2000) also incorporate conceptual models to avoid time-demanding numerical calculations. We will give an overview of some expert systems in Sect. 4.

3 QPF algorithms

3.1 Cell tracking algorithms

3.1.1 TITAN (3D)

Amongst the numerous cell trackers described in the literature, the TITAN algorithm (Thunderstorm Identification Tracking Analysis and Nowcasting; Dixon and Wiener, 1993) is most widely used in meteorological services worldwide. TITAN works on volumetric radar data in Cartesian coordinates. The storm *detection* is quite straightforward: a storm is defined as a contiguous region of enhanced reflectivity exceeding a certain threshold in both reflectivity (T_Z) and volume (T_V). The thresholds are fixed throughout the analysis and typical values are $T_Z = 35\,\text{dBZ}$ and $T_V = 50\,\text{km}^3$. In each volume scan, an inventory is made of all storm cells, and for each cell a number of properties is derived. The ones that are important for the cell tracking algorithm are the reflectivity-weighted centroid ($\bar{x}$, $\bar{y}$, $\bar{z}$), the volume V, and the size and shape of the storm area. The shape is approximated by an ellipse fitted to the projection of the storm on the horizontal plane. The storm cell *tracking* (Fig. 5) is made through a combinatorial optimisation. Given two volume scans at time t_1 and t_2 (= $t_1 + \Delta t$), all possible paths between the storm cells are considered. A track is favoured as a "true one" if it is shorter, and if it connects storm cells with similar properties. Mathematically, this translates in the minimisation of a cost function $\sum C_{ij}$, with for each combination (possible paths) of storms $\mathbf{S}_i(t_1)$ and $\mathbf{S}_j(t_2)$ with centers $(\bar{x}_i, \bar{y}_i)$ resp. $(\bar{x}_j, \bar{y}_j)$:

$$
\begin{aligned}
C_{ij} &= w_1 d_p + w_2 d_V \\
\text{where} \quad d_p &= [(\bar{x}_i - \bar{x}_j)^2 + (\bar{y}_i - \bar{y}_j)^2]^{1/2} \\
d_V &= |V_i^{1/3} - V_j^{1/3}|
\end{aligned}
$$

Here, d_p is a measure of the distance moved, while d_V a measure of the difference in volume; w_1 and w_2 are weights. An additional constraint is set on d_p, as this distance cannot exceed the distance given by the maximum storm speed. The final paths are then given by the minimisation of $\sum C_{ij}$.

A third component of the algorithm, besides the detection and tracking components, is the *handling of mergers and splits*. For mergers, the algorithm searches for storm tracks that are terminated. If the forecast vector of such a terminated path at t_1 is lying in the projected area of a storm at t_2, then it is concluded that the storm did not terminate, but merged to form the t_2 storm. For splits, the algorithm searches for storm tracks at t_2 that have no history. If the centroid of such a storm is lying within a forecast ellipse of a storm at t_1, then it is concluded that the storm is not a new one, but that a split has taken place.

A storm *forecast* is given by the extrapolation of not only the storm position, but also of the other storm properties as e.g. the volume (and hence TITAN does not deliver a persistence forecast). The extrapolation for a parameter p is made on the basis of a certain number of previous values of this parameter, with exponentially decreasing weights further back in time. The forecast of the storm area as given by the area of the ellipse, is derived from the extrapolation of the storm volume, since the latter one varies more smoothly than the area itself. The aspect ratio and the orientation of the ellipse are kept constant in this extrapolation.

Known weaknesses of the TITAN algorithm are the fact that the shape approximation by an ellipse is not always valid, and that the single threshold does not allow for a flexible detection. Also, it should be investigated whether the typical values for T_Z and T_V are valid for the region for which TITAN is used. In the newer versions of TITAN, the shape approximation by an ellipse is replaced by an approximation by a polygon. This polygon is computed by projecting radials out from the storm centroid and finding the intersection point with the storm boundary.
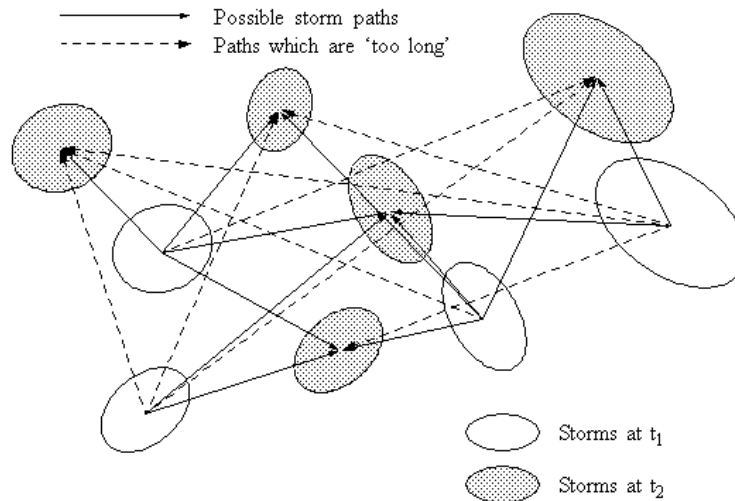
Figure 5: Storm tracking in TITAN is done through an optimisation evaluating every possible track between the storms (see text for details). Figure taken from the TITAN website WWW.RAP.UCAR.EDU/PROJECTS/TITAN/, originally published in Dixon and Wiener (1993).

Nowadays, the TITAN cell tracking algorithm is part of a larger software package with the same name. The TITAN package is an entire software system that does not only support storm tracking and forecasting, but also a variety of tasks like merging individual radars into a mosaic, removal of clutter and anomalous propagation, bright band correction, etc... The system is freely downloadable (for research purposes) from WWW.RAP.UCAR.EDU/PROJECTS/TITAN/. The TITAN system is used operationally in several meteorological institutes.

3.1.2   SCIT (3D)

Another widely used cell tracking algorithm for volumetric radar data is SCIT (Storm Cell Identification and Tracking; Johnson et al., 1998). The major difference between TITAN and SCIT is that the latter algorithm works with several (default is seven) reflectivity thresholds for the cell detection. Another difference is that cell tracking is not done through a combinatorial optimisation, but solely upon a distance criterion. To match a certain cell at time t_2 ($= t_1 + \Delta t$) with a cell observed at time t_1, the position of the current cell (at t_2) is compared with the predicted positions of all cells of t_1, based upon their velocity as deduced from previous scans. The cell at t_2 is then matched with the cell at t_1 for which its predicted position is closest to the cell at t_2.

Another novelty introduced by Johnson et al. (1998) is the concept of a *cell-based VIL*. In the calculation of a cell-based VIL, the maximum reflectivity value within a storm is taken at each level, and then these maxima are vertically integrated through the depth of the storm. Cell-based VIL takes into account that storm volumes can be vertically tilted. It is also introduced with practical considerations, since cell-based VILs can easily be added to the other storm cell characteristics, contrary to grid-based VIL values.

Following Johnson et al. (1998), SCIT performs very well as a tracker for convective cells, but largely fails in tracking mesoscale stratiform precipitation areas. For these situations, the authors acknowledge area trackers to be more suitable. SCIT is not freely downloadable, but it is integrated in the WDSS-II system (WDSS-II: see Sect. 4.16.5).
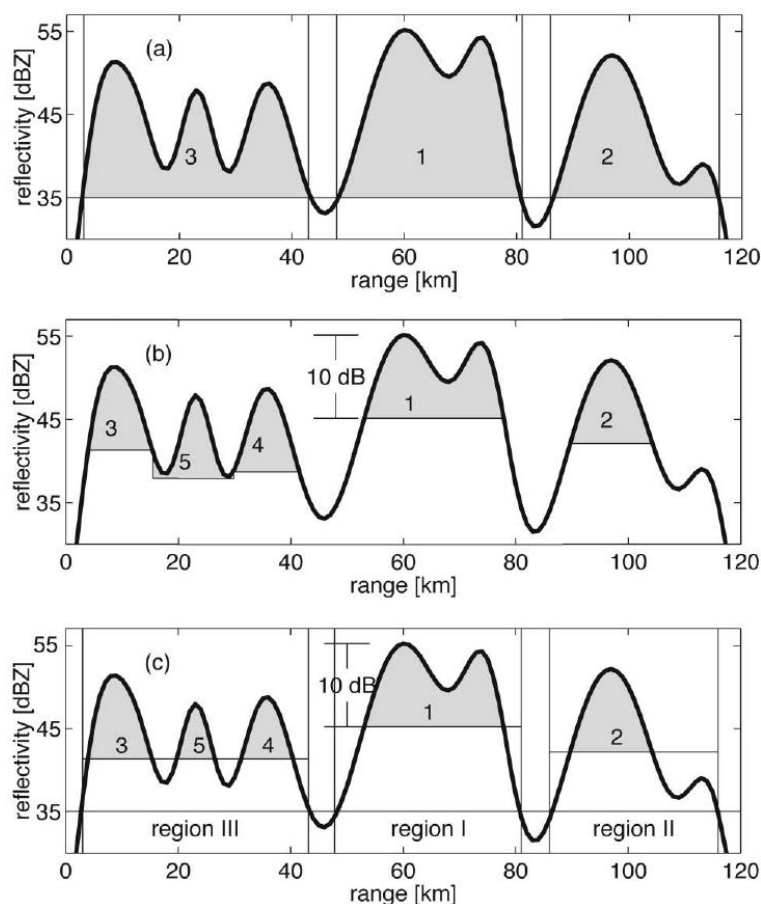
Figure 6: Illustration of three different cell detection algorithms. In the *upper panel*, a single threshold is used (as in TITAN), often leading to an inadequate cell detection: the detected cells can consist of multiple cells. In the *middle panel* (b), a single, but *relative* threshold is used: the area of 10 dBZ around each local maximum is defined as a cell. This technique leads to cells that "grow" into other cells, as can be seen from cell 5 on the figure. The technique used in TRACE3D is illustrated in the *lower panel* (c). The detection has two steps: first, contiguous regions above a certain (low) threshold are detected (regions I to III in the figure). Within each region, a second (relative) threshold is used, 10 dBZ beneath the maximum reflectivity value *of that region*. This RC "depth" of 10 dBZ is in fact a free selectable parameter of the algorithm, but its default value is 10 dBZ. Figure taken from Handwerker (2002).

3.1.3 TRACE3D (3D)

A third cell tracking algorithm for volumetric data which we discuss here is TRACE3D developed by Handwerker (2002). It contains some innovative features in both the identification and the tracking of storm cells. The cell *detection*, illustrated in the lower panel of Fig. 6, consists of two stages. First, a rough division is made of the reflectivity field into *regions*, based on a single threshold (default 35 dBZ). Then, the regions are subdivided into the final cells (*reflectivity cores RCs* as they are called in TRACE3D) by a second threshold, which is equal to the maximum reflectivity value within that region minus 10 dBZ. This RC "depth" of 10 dBZ is in fact a free selectable parameter of the algorithm, but its default value is 10 dBZ.

The *tracking* procedure resembles the one in SCIT, but has some important differences in the way it handles cell splitting and merging. In a first stage, the algorithm estimates the position

of a cell, based on its position in the previous scan and on an estimated velocity, and defines a certain search radius around this position. The cells of the current scan lying within this radius are potential "children" cells. These candidate children cells are then further checked for possible splits and merges. This is done by comparing the size of the parent and child cells; if their sizes are different by some predefined factor, then splitting is assumed, and the algorithm searches for (an) extra child cell(s) in the vicinity of the first child. Merging is done in the same way, but with the two scans reversed in time.

Finally the tracks are scanned for possible track *crossings*. A track crossing is defined here as the crossing of the routes of two different cells in two consecutive scans. Although such crossings are not impossible (the two cells can pass a crossover point on a different moment between two consecutive scans), they are highly unlikely. Such crossings are removed by removing the less probable parent-child identifications (less probable in the sense of the direction of the track compared to the global flow direction).

The performance of TRACE3D has been evaluated against test persons. It turned out that TRACE3D performed slightly worse than the human eye, especially in situations with a complex cell pattern. Nevertheless, TRACE3D reaches a Critical Success Index (CSI) of on average 91 % on images with a 5 min resolution. The algorithm is available as source code for free, upon request to the author.

3.1.4 CELLTRACK (2D MAX field)

The operational QPF system at the Czech Hydrometeorological Institute (CHMI) is based on the area tracker COTREC (see Sect. 3.2; Li et al., 1995), combined with wind fields of the NWP model ALADIN (see Sect. 4.4; Novák, 2007). Generally, this system is appreciated by the forecasters, but in convective situations the nowcasts are less accurate, especially when the movement of individual cells deviates from the larger storm complex displacement. For these situations, the CHMI developed an additional cell tracking algorithm: CELLTRACK (Kyznarová and Novák, 2005, 2007; Novák and Kyznarová, 2006). Both the COTREC and the CELLTRACK forecasts are operationally available to the forecasters in one visualisation environment.

For the *cell identification*, the CELLTRACK algorithm uses a single threshold, with a default value of 44 dBZ on the maximum reflectivity field (2D field). The authors Novák and Kyznarová justify the choice for this simple detection method by claiming that more sophisticated algorithms with adaptive thresholding for identification have a lower performance in cell tracking. The claim is based on a comparison of the performance of CELLTRACK against the TRACE3D algorithm (TRACE3D: see Handwerker, 2002, or Sect. 3.1.3). Another argument for a single detection threshold is from an operational point of view: it is important to predict movement of areas of high reflectivity instead of only reflectivity peaks.

The *cell tracking* part of the algorithm is much more complex. The assignment between parent and child reflectivity cores passes through an intermediate level, in which all potential parent-child cells are grouped into cell *clusters*. This intermediate level has to facilitate the cell tracking in case of crowded cell complexes. The tracking of two sets of cells, a set at time t_1 and a set at time t_2 (= $t_1 + \Delta t$), consists of the following steps:

1. Cells at time t_1 are translated to time t_2, using the COTREC velocity field. Real cells at time t_2 that are lying within a certain distance of the translated cells are marked as possible children of these cells. A similar procedure is done on the cells at time t_2, but backward in time: real cells at time t_1 are marked as possible parents of the cells at time t_2. All cell connections obtained by these two procedures form the cell cluster.

2. The parent-child assignments are made on the level of the cell clusters. For each potential parent-child pair, a shape similarity measure sim is calculated in a rectangle containing the

pair:

$$sim = \frac{YY + NN}{YY + YN + NY + NN}$$

in which YY is equal to the number of pixels occupied by both reflectivity cores, NN is equal to the number of unoccupied pixels in the rectangle and YN and NY are pixels occupied by only one reflectivity core. Parent-child assignments are then realised using certain criteria of this shape similarity measure and of the distance (for more details on these criteria, see Kyznarová and Novák, 2005).

3. Splitting and merging of cells are treated as in the TITAN algorithm.

For the cell *extrapolation*, a motion vector is defined for mutually assigned cells. For this vector, not the connection of the geometrical centers is taken, but the vector $\mathbf{v}$ realising the minimum of the expression

$$n \sum_{n \in X} |Z_p^\star(n) - Z_{ch}(n)|$$

where X is the area covered by united parent(s) and child(ren) areas and n is the number of pixels covered in this area. In this area, reflectivity values from the child(ren) at t_2 (Z_{ch}) are subtracted from the reflectivity values from the parent(s) at time t_1 (Z_p) translated by $\mathbf{v}$ (noted $Z_p^\star$). This vector is then used to extrapolate the cell.

The *verification* of the algorithm has been rather limited. The cell tracking was evaluated against a manual tracking, but only four days of data were considered for evaluation. The forecast skill was estimated by comparing the CELLTRACK extrapolation with (Eulerian) persistence and the COTREC forecast. CELLTRACK was found to be much better (CSI score) than persistence, but only marginally better than COTREC.

3.1.5   TRT (2D MAX field)

A last tracking algorithm we will discuss is the Thunderstorm Radar Tracking algorithm (TRT; Hering et al., 2004, 2005, 2006). TRT is the operational nowcasting tool of MeteoSwiss, and hence it will be discussed in more detail in Sect. 4. Here, we only describe the cell detection and tracking part, as described in Hering et al. (2004). Similar to TRACE3D, it uses an adaptive thresholding scheme, allowing cells to be detected and tracked in different stages of their evolution. The cell *detection*, which is illustrated in the *upper panel* of Fig. 7, does not work on volumetric data, but on the maximum reflectivity field. Three different reflectivity thresholds are involved in the scheme: dB_{th}, dB_{min} and ΔdB_T. For each cell detected by TRT, the difference between the maximum reflectivity value in that cell and the value at the base of the cell must be at least ΔdB_T. The lowest possible reflectivity value (but greater than a fixed value dB_{min}) *that allows it to distinguish this cell from nearby cells*, is taken as the detection threshold dB_{th}. The default values for the operational TRT system are $dB_{min} = 36$ dBZ and $\Delta dB_T = 6$ dBZ. From Fig. 7 it is clear that such an adaptive threshold scheme is able to detect cells at different stages of development: more mature cells have a higher threshold dB_{th}.

The cell *tracking* is illustrated in the *lower panel* of Fig 7. A cell on two consecutive volume scans is identified as the same object, if the cell on the current scan has a large enough overlap (in area) with the cell of the previous scan *translated to the current time* using a velocity estimate. Also cell splitting and merging is taken into account in this manner. Small cells are artificially enlarged to ensure overlap for the tracking procedure. Case studies reveal a satisfactory performance of the algorithm, but it fails in cases of a frontal passage and slowly moving cells. The more recent versions of TRT (Hering et al., 2005, 2006, 2008) solve this issue, and contain also several other improvements. These improvements will be discussed in Sect. 4.15.
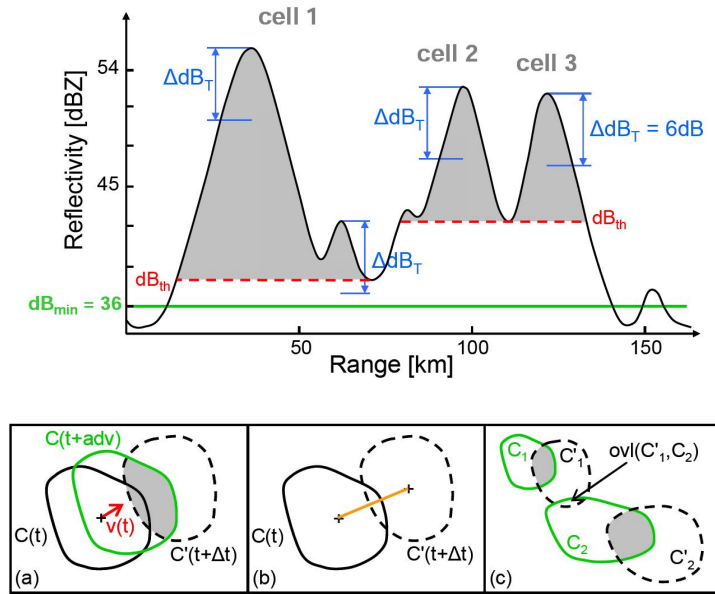
Figure 7: Illustration of the detection (*upper panel*) and tracking (*lower panel*) of the Thunderstorm Radar Tracking (TRT) algorithm. The detection is based on an *adaptive* threshold scheme (see text for details); the tracking of a cell observed at time t (cell C) and at time t+Δt (cell C') is based on the area overlap between cell C' and cell C translated to time t+Δt, noted C(t+adv). Figure taken from Hering et al. (2005).

3.2 Area tracking algorithms

Pioneering area tracking algorithms date from the early sixties (e.g. Hilst and Russo, 1960). In this early phase, the movement of the entire image was modeled by one single vector, namely the translation vector realising the highest correlation between two consecutive images. The next logical step was then to break up the radar field into smaller entities, and calculate a vector *grid* between two consecutive images.

3.2.1 TREC and COTREC

The first implementation of the area tracking principle was done by Rinehart and Garvey (1978) in their TREC algorithm. The concept is already explained in Sect. 2.2. In their simplest form, tracking algorithms produce quite noisy and even erroneous velocity fields. Therefore, a "raw" TREC field is not applicable directly, and some smoothing or correction process has to be considered. Several of these post-processing techniques have been proposed, the most well known being COTREC (COntinuity of TREC vectors; Li et al., 1995). This technique was already explained in Sect. 2.1, in the context of the optical flow technique. It consists of reprocessing the raw TREC velocity field $\mathbf{v}(u, v)$ through a minimisation of $\partial u/\partial x + \partial v/\partial y$. The technique was tested by the comparison of the radial component of the velocity field with Doppler velocities, yielding an significant improvement compared to TREC vectors. In the COTREC scheme, a very rudimentary echo growth and decay estimate is made, just by comparing the total reflectivity of a box with the corresponding box in the previous image.

COTREC has been extensively verified and optimised by Mecklenburg et al. (2000). The quality of the COTREC forecast was studied by the commonly used quality checks like POD, CSI and FAR (see the short note on verification statistics at the end of this document, p. 52). These results were then applied in the optimisation of the forecast scheme. For example, a sig-
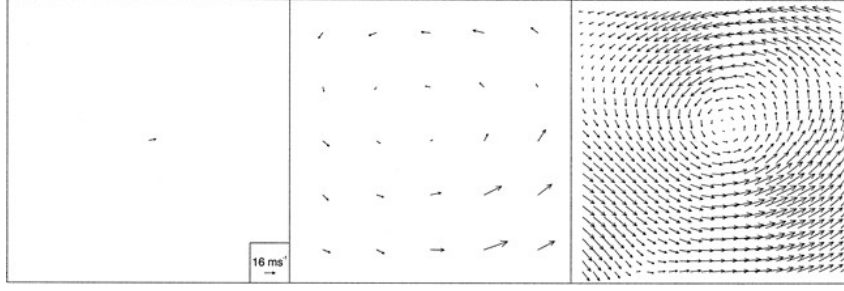
Figure 8: Scaling guess procedure in the VET method: the box size for the velocity grid is gradually decreased. This is done to avoid convergence towards local minima for the velocity field. Figure taken from Germann and Zawadzki (2002).

nificant improvement of the procedure is obtained by a spatial smoothing of the field before the actual correlation calculation, and by fine-tuning the number of correlation boxes. COTREC has a commercial version called RainCast (Schmid et al., 2000); the validation of this product was done in Schmid and Wüest (2005). The latest version, RainCast+ (Schmid et al., 2002), is also aimed at forecasting snowfall and freezing rain, but the validation was limited to a (qualitative) study of only a few specific cases.

3.2.2 VET (MAPLE)

Another, somewhat more sophisticated area tracking algorithm is the VET (Variational Echo Tracking) method, as part of the McGill Algorithm for Precipitation Nowcasting Using Semi-Lagrangian Extrapolation (MAPLE, Sect. 4.8). The algorithm was originally developed by Laroche and Zawadzki (1994) to retrieve three-dimensional wind fields from single-Doppler clear-air echos. Germann and Zawadzki (2002) adapted it to determine the velocity field of continental-scale radar composites. The velocity field $\mathbf{v}(u, v)$ for a radar domain Ω is determined by a global minimisation of the cost function J_{VET}:

$$J_{\mathrm{VET}}(\mathbf{v}) = J_Z + J_2 \tag{4}$$

with

$$J_Z = \iint_\Omega \beta(\mathbf{x})[Z(t_0, \mathbf{x}) - Z(t_0 - \Delta t, \mathbf{x} - \mathbf{v}\Delta t)]^2 dx dx$$

and

$$J_2 = \gamma \iint_\Omega \left(\frac{\partial^2 u}{\partial x^2}\right)^2 + \left(\frac{\partial^2 u}{\partial y^2}\right)^2 + 2\left(\frac{\partial^2 u}{\partial x \partial y}\right)^2 + \left(\frac{\partial^2 v}{\partial x^2}\right)^2 + \left(\frac{\partial^2 v}{\partial y^2}\right)^2 + 2\left(\frac{\partial^2 v}{\partial x \partial y}\right)^2 dx dy$$

J_Z is in fact the square of the residuals of the advection equation (Eq. 2), with an additional weighting factor $\beta(\mathbf{x})$ representing the data quality. Z is the radar reflectivity field as usual (preferentially in dBZ). The second term of Eq. 4, J_2, is added to ensure smoothness of the resulting velocity field. γ is a constant weight. The two variables u and v are obtained in a global minimisation of this nonlinear cost function.

Germann and Zawadzki (2002) point out that a reliable initial guess is needed to avoid that the minimisation of J_{VET} converges towards a local minimum. This initial guess is obtained by iteratively increasing the grid resolution of the radar domain. The procedure starts with one velocity vector for the whole domain, and then the box size determining the grid resolution is gradually decreased. This technique is illustrated in Fig. 8.

4   Operational and research QPF systems

Operational nowcasting systems come in a variety of versions. Some of them only focus on precipitation, others on a variety of meteorological parameters like e.g. fog, cloud cover, temperature, etc...If a system deals with more than only precipitation, we will limit our discussion to the precipitation aspect only. Some systems are quite transparent, merely consisting of an implementation of an algorithm presented in Sect. 3; others are complicated systems incorporating different data sources and complex merging schemes. The scope of this section is somewhat broader than only the *operational* systems; we will discuss also several extensions of existing systems that were solely developed as research tools.

QPF systems are developed for a specific *radar configuration*, a specific *geographical region* with its own orography, and for specific *user requirements*. Therefore, the skills of two different operational nowcasting systems cannot be compared. One effort to compare different (operational and research) nowcasting schemes was done in Sydney in 2000, known as the Sydney 2000 Forecast Demonstration Project (Wilson et al., 2004; Pierce et al., 2004). During nearly three months, the systems were run at the Australian Bureau of Meteorology (BoM). Systems involved were TITAN, NIMROD, GANDOLF, ANC, S-PROG (CARDS and WDSS were also involved, but were not designed specifically for precipitation forecasting). The general conclusion of this experiment was (from Pierce et al., 2004): "*..., nowcasting algorithms based upon the linear extrapolation of observed precipitation motion (Lagrangian persistence) were generally superior to more sophisticated, nonlinear nowcasting methods. Centroid trackers (TITAN) and pattern matching extrapolators using multiple vectors (Auto-nowcaster and Nimrod) were most reliable in convective scenarios. During widespread, stratiform rain events, the pattern matching extrapolators were superior to centroid trackers and wind advection techniques (Gandolf, Nimrod).*" A similar forecast demonstration project was organised for the recent Olympic Games in Beijing (e.g. Joe et al., 2008, see also www.b08fdp.org). Systems involved there include ANC (Chinese variant), CARDS, SWIRLS, STEPS, TIFS,...A new element in the project is the real time forecast verification to intercompare the QPF results, led by dr. Elizabeth E. Ebert (BoM, Australia). Publications on the results of this project are expected to appear soon.

In the following pages we will describe a few nowcasting systems. The selection of the systems we discuss is certainly biased towards the ones that are described in the literature. The systems are discussed in alphabetical order.

4.1   AMV system – Finland

Main reference: Hohti et al. (2000)
The operational Finnish nowcasting system is based on an adaptation of the Atmospheric Motion Vector (AMV) system developed by EUMETSAT. The AMV system is an area tracker; the basic setup is similar to TREC (Section 3.2). The five latest 500 m pseudo-CAPPI reflectivity fields are ingested in the AMV system. The generated vector field is quality controlled, smoothed, and interpolated for the non-precipitating areas. The future rainfall at a specific point is calculated by the reversed trajectory, taking into account the inaccuracies along the trajectory. As doing so, the future precipitation on a specific point is based on a weighted average of the rain rate inside an ellipse on the latest rainrate field (Fig. 9). Verification of the method proved that the forecast quality is satisfying, but that the method fails when only a few rain cells are present on the images.

The use of optical flow (OF, Sect. 2.1) was recently studied at the Finnish Meteorological Institute, as an alternative for the AMV autocorrelation method (Peura and Hohti, 2004, 2005). The optical flow constraint (OFC) they propose was already discussed in Sect. 2.1. Some additional tweaking is necessary for OF to be operationally applicable: (a) a smoothing of
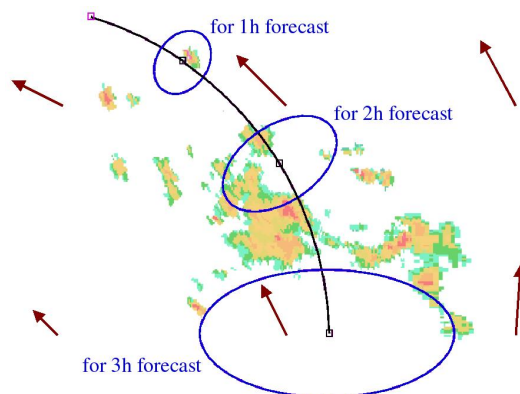
Figure 9: In the AMV system (Hohti et al., 2000), the future precipitation on a specific point is calculated from a weighted average of the rain rate inside an ellipse on a previous image.

the rain field has to be done before the derivatives of Eq. (2) can be calculated; (b) some numerical acceleration techniques are implemented; and (c) quality information is extracted from the OF method and used in further steps. Peura and Hohti (2005) conclude that OF is a good alternative for the computationally heavy area tracking methods.

4.2   ANC Auto Nowcast system – U.S.A.

Main reference: Mueller et al. (2003)
Amongst all nowcasting systems worldwide, the Auto Nowcast system of the National Center for Atmospheric Research (NCAR, U.S.A.) is definitely the most complex one. A number of different data sources is ingested in the system, for example: radar reflectivity and doppler scans, satellite images, mesonet weather station data, soundings, etc. . . The data flow passes through respectively (1) *analysis algorithms* that convert the input data to 14 *predictor fields*; (2) a fuzzy logic algorithm that converts the predictor fields into *likelihood fields* using *membership functions*; and (3) the construction of a *final likelihood field* as the nowcast. A schematic overview of the procedure is given in Fig. 10.

The *analysis algorithms* are a collection of algorithms, each of them responsible for a specific part of the data flow. TITAN (Sect. 3.1) and TREC (Sect. 3.2) are used (amongst others) to define 5 different predictor fields, like e.g. the extrapolated reflectivity. Other algorithms concentrate on the satellite data, and produce for example the cloud top temperature predictor field. In the next step, the predictor fields are converted into likelihood fields using membership functions. These membership functions are functions that reach values between -1 and 1, and represent the relative importance of a predictor field value to the final forecast. In other words, they indicate for which values a predictor field becomes important for the final forecast. The constructed likelihood fields are combined using fixed weights, and this combined likelihood field is then smoothed and thresholded to form the final nowcast.

Boundary layer convergence lines (or *boundaries* in short) play an important role in the whole system. Boundaries are defined here as "narrow zones of boundary layer convergence associated with weather phenomena such as gust fronts, sea-breeze circulations, terrain-induced circulations, horizontal convective rolls, and synoptic-scale fronts". They play a crucial role in the development of convective storms. ANC contains a dedicated algorithm "COLIDE" to automatically detect these boundaries, and extrapolate them for the nowcast. This feature of ANC should make it possible to predict storm initiation, which is beyond the capabilities of any pure extrapolation algorithm. An example of a successful storm initiation prediction is shown in
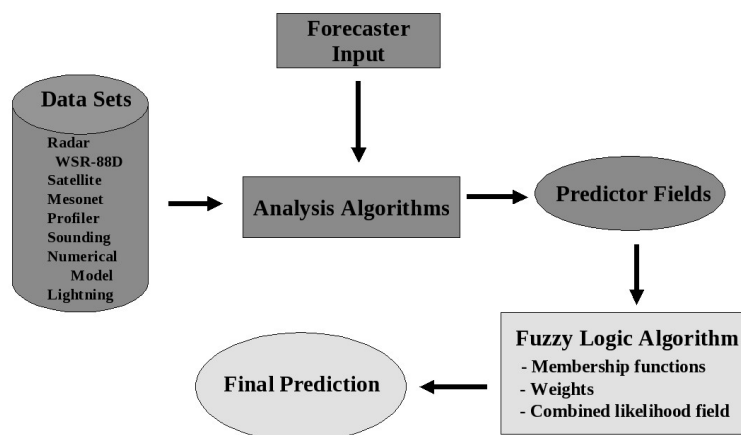
Figure 10: Schematic overview of the ANC system (see text for discussion). Figure adapted from Mueller et al. (2003).
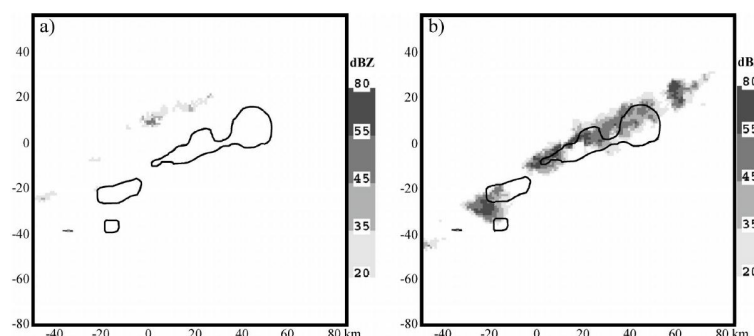

Figure 11: Example of a successful prediction of a storm initiation by ANC. The *left panel* shows the radar reflectivity field (grey scale) on the issue time; the *right panel* shows the reflectivity at verification time (30 minutes later). The contours on each panel is the ANC nowcast at issue time. Figure from Mueller et al. (2003).

Fig. 11. The boundaries are, however, not always successfully detected, and often forecaster inputted boundaries are required to make correct predictions.

4.3 CARDS – Canada

Main reference: Donaldson, priv. comm.
CARDS (Canadian Radar Decision Support) is the nowcasting system of the Meteorological Service of Canada. It is one of the nowcasting systems that participated in the Sydney 2000 Forecast Demonstration Project, and more recently in the Beijing 2008 Forecast Demonstration Project. CARDS is an advanced expert system, but unfortunately, it is scarcely documented in the literature. The system includes a cell based approach, modelled on TITAN (Sect. 3.1.1), with modifications for the Canadian climate(s), and an advection forecast that has evolved from the McGill SHARP program (the predecessor of MAPLE, see Sect. 4.8 for more details). The first goal of CARDS is to provide guidance to human forecasters, by doing computationally intense tasks of deriving predictors from the data. These predictors, such as extrapolated radar patterns, mesocyclonic patterns, shear, etc...are presented to the forecaster who uses them to quickly focus on meteorologically important features.

One useful feature that CARDS inherited from SHARP (Bellon and Austin, 1978) is the concept of "most probable" forecast and "worst case" forecast. When doing the extrapolation forecasts for point locations, CARDS produces as output both the values directly along the motion vector and also the maximum echoes in a sector on either side of the motion vector. In a sense this is a low-order, crude precursor to "statistical" forecasts: presenting both the expected values and a sense of uncertainty. This method is computationally cheap and avoids the issue of re-introducing synthetic small scale information (scaling/normalisation/energy cascades) such as in S-PROG (Sect. 4.11) and other forecast systems that smooth the explicit forecast with time.

4.4   Czech system

Main reference: Novák (2007)
The nowcasting system developed by the Czech Hydrometeorological Institute (CHMI) makes use of the area tracking algorithm COTREC (Sect. 3.2) and the NWP model ALADIN. Wind fields at 700 hPa are extracted from ALADIN, and compared to the velocity field generated by COTREC. Both velocity fields are only compared, and not blended. It is concluded that COTREC velocity fields are slightly more reliable than ALADIN wind fields to predict rain field motion. Fine tuning the COTREC parameters is acknowledged to be very important to improve the quality of the prediction. However, both methods fail in cases of convective storms with cell velocities different from the larger storm complex. The use of the ALADIN wind field as a first guess for the motion field calculation in the COTREC algorithm is currently being developed at CHMI (Novák et al., 2008).

Especially for these convective situations, the cell tracking algorithm CELLTRACK was developed recently (see Sect. 3.1; Kyznarová and Novák, 2005; Novák and Kyznarová, 2006). Its output is available to the forecasters in the same visualisation environment as the COTREC output. Tracks of the detected cells are shown, together with an extrapolation for 30 min ahead. CELLTRACK was found to produce slightly better forecasts than COTREC in convective situations. CELLTRACK was also used at CHMI to perform a climatological study of convective cells between 2002 and 2006 (Kyznarová and Novák, 2007). Statistical studies were made for cell lifetime, cell area, altitude of maximum reflectivity and echo top heights.

4.5   GANDOLF – U.K.

Main reference: Pierce et al. (2000)
GANDOLF is designed as an alternative nowcasting system for NIMROD (Sect. 4.9) in cases of air mass convection. It is developed by the U.K. Met. Office for the Thames area, mainly for hydrological applications (flood prediction). GANDOLF consists of three levels of operation. The *first level* receives the radar scans, and examines if any precipitation is being observed in the region of interest. If precipitation is observed, GANDOLF activates its *second level*. In this level, the system verifies if air mass convection is present. If not, then the nowcast is further handled by the NIMROD system. If there is air mass convection, then the core of GANDOLF, the Object-Oriented Model (OOM, see below) is run. In the case of a forecast of severe precipitation, *level three* is activated, the alert status, in which warning messages are sent to the users.

The OOM is the core of the GANDOLF system. In this model, each convective cell is treated as an individual entity. The stage of evolution of each cell is compared to a *conceptual model* of a convective cell. A conceptual model of a physical phenomenon is interpreted here as a model for the evolution of that phenomenon, without a full description of the physics behind that phenomenon. Using conceptual models, one can skip intensive numerical calculations and

thus gain significantly in forecast calculation speed. The conceptual model for a convective cell that is used in GANDOLF is that proposed by Hand and Conway (1995). This model divides the evolution of a storm cell into six different stages (young developing, developing, young mature, fully mature, early dissipating and dissipating). Together with a detailed description of the different stages, also an identification process is given in Hand and Conway (1995). With this process, it is possible to determine the stage of evolution of a cell for a given radar observation of that cell.

Note that the conceptual model that is integrated in GANDOLF, is not valid in cases of organised convection, during for example frontal zones. In those cases, GANDOLF is not run, and the NIMROD output is used. Whether the right conditions are met to run either GANDOLF or NIMROD, is verified using several criteria, including for example near-surface CAPE (Convective Available Potential Energy).

Unlike ANC, GANDOLF is not designed to predict storm *generation*; it is designed for an early detection of very young precipitation cells and the prediction of their future development. Concerning the verification, GANDOLF has proven to be a reliable nowcasting system, but still further work has to be done. For example, one known flaw is the pulsing behaviour of some cell evolution forecasts. Another weak point is the advection of the cells, which is based (at least in the version of Pierce et al., 2000) on steering level wind vectors from a mesoscale NWP model. Recently, Bowler et al. (2004b) have investigated if this inaccurate advection method could be replaced by an optical flow scheme. This study is discussed in the next section.

4.6 GANDOLF + OF – U.K.

Main reference: Bowler et al. (2004b)
The advection in the operational GANDOLF system (Pierce et al., 2000) is either derived from the wind vectors of a mesoscale NWP model, or it is based on a cross-correlation area tracker. Contrary to TREC (Sect. 3.2), the GANDOLF area tracker does not track on a rectangularly partitioned field, but performs a correlation on the detected *contiguous rain areas* (CRAs). Bowler et al. (2004b) verified if this advection could be replaced by an optical flow (OF) scheme. The basics of OF, as well as the particular OFC used in this GANDOLF version, were already discussed is Sect. 2.1. The verification of the OF scheme through both a few case studies and with verification statistics, points to an overall better performance of this scheme compared to the operational system, especially for lead times around one hour. Particularly, the OF scheme is superior in cases of embedded convection and differential precipitation motion.

4.7 INCA and GaliMet – Austria

Main reference: Haiden et al. (2006) for INCA and Auer et al. (2007) for GaliMet
Two independent nowcasting systems are currently developed at the Central Institute for Meteorology and Geodynamics (Zentralanstalt für Meteorologie und Geodynamik, ZAMG) in Vienna, Austria: INCA and GaliMet.

The scope of the INCA system is very broad: it produces nowcasts not only for precipitation, but also for temperature, humidity, wind, cloudiness and snowfall. The precipitation forecast is an advection based forecast for the first two hours, and is then gradually converted to the NWP precipitation forecast (a combination of ALADIN and ECMWF output is used). The motion vectors are derived from consecutive precipitation analyses and filtered by a comparison with ALADIN vectors. Unfortunately, no further details on the specific procedure are given. The INCA system is an ambitious project still under strong development. The current version contains some assumptions and methods that still have to be refined. The authors are aware of

this fact, but preferred to implement a basic version first, and then further refine and integrate the whole system.

GaliMet is a system that focusses on analysis and warnings of severe weather alone. It ingests radar images as the primary data source, supplemented with lightning data and satellite images. The cell detection is done through one single threshold on the maximum reflectivity field. Cells on consecutive radar images are identified by means of their overlap area (similar to the TRT algorithm, Sect. 3.1.5). Cells are extrapolated on the basis of the previous positions of their centroids. Together with this extrapolation, also a V-shaped warning sector is calculated, indicating the most likely future locations of the cell. The size of the opening angle of this V-shaped region depends on the steadiness of past displacement of the cell. Radar cells are identified (with increasing hazard) as "showers", "thunderstorms" (lightning present in the cell) or "severe" (hail present).

A unique feature in GaliMet is that in the case that the radar data are unavailable, satellite data are used as an alternative. More precisely, METEOSAT-9 images are used (water vapour band, IR 10.8 μm and IR 12.0 μm). From these images, two derived products (precipitation estimate and cloud top height) are further processed, and downscaled to the radar resolution. Cells are extrapolated and warning sectors are calculated, similar to the radar procedure (except that the warning sectors are now cylindrically shaped). GaliMet has been verified during one month, July 2006, and it was concluded that the warnings of up to 45 min were sufficiently reliable, with a slight underestimation of heavy precipitation ("showers"), while "thunderstorms" and hail shower warnings ("severe") are issued too often. GaliMet is in fact developed in collaboration with a private company, which is responsable for commercialising the warnings through an SMS service. The idea is to customise the warnings depending on the position of the user by GPS information.

4.8   MAPLE – Canada

Main reference: Germann and Zawadzki (2002)
Commercialised version: HDSS, Conway and Eilts (2004)
MAPLE is the acronym for the McGill Algorithm for Precipitation Nowcasing Using Semi-Lagrangian Extrapolation. It is a QPF algorithm developed by the renowned radar group of the McGill University (Montreal, Canada). The algorithm has been under constant development since the early seventies (SHARP, Austin and Bellon, 1974; Bellon and Austin, 1978) up to now. The current status of the MAPLE algorithm is described in a recent series of four papers from the authors Germann, Zawadzki and Turner. The papers are an excellent review-like introduction to the basic concepts of QPF (Lagrangian persistence, perishability of small scales), but offer at the same time an in-depth study of these concepts. Note, however, that the papers are aimed at a continental-scale QPF, using very large radar composites with a relatively coarse resolution. Although the principles and concepts are certainly valid for smaller domains, the data and parameters in this study are not optimised for very short term forecasts based on radar images at full resolution.

The main objective of **Paper I** of the series (Germann and Zawadzki, 2002), apart from the introduction of the main concepts, is to study the *lifetime* of precipitation patterns and, more precisely, the *scale dependance* of this lifetime. It is common sense that small precipitation features have a shorter lifetime than large ones, but to what extent? And how can this be quantified? Germann and Zawadzki (2002) argue that predictability should be quantified relative to a certain forecasting method. In short, the procedure outlined in this paper consists of three parts: (i) the velocity field is determined through Variational Echo Tracking (VET, see Sect. 3.2.2); (ii) the rainfield is advected by Lagrangian persistence; and (iii) the advected field is compared with the observed field. This procedure can be repeated for *decomposed* rainrate
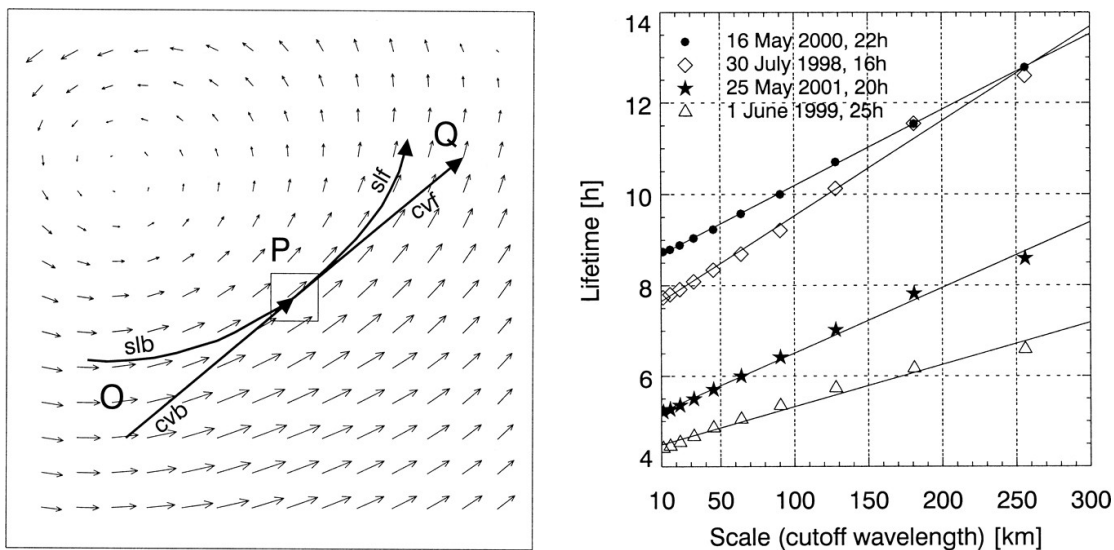
Figure 12: *Left panel*: Lagrangian advection can be realised in four different schemes. In a forward scheme (SLF, CVF) reflectivity or rainrate is advected forward in time, while in a backward scheme (SLB, CVB) the rain rate in P is determined from a parcel O back in time. In both schemes, the actual displacement can be the (constant) vector at point P (CVF, CVB) or can follow the vectors along the velocity field (SLF, SLB). *Right panel*: Final result of Germann and Zawadzki (2002): the lifetime of precipitation features for four different events increases linearly (on a logarithmic scale) with the dimension of the features. Both figures from Germann and Zawadzki (2002).

fields, in order to determine the scale dependance of predictability of the precipitation features. For the Lagrangian advection, four schemes are proposed, illustrated in the *left panel* of Fig. 12. In this figure, P is the grid point of interest for which the future rainrate will be determined. This can be done either through a *backward scheme*, in which the rain rate in P is determined from a parcel O that would end up at grid point P (similar to AMV, Fig. 9), or through a *forward scheme*, in which the reflectivity or rainrate is advected to a parcel Q. Of course, neither O or Q coincide exactly with a grid point, and hence in a backward scheme, the value in O is obtained by interpolation, while in a forward scheme, the value in P is redistributed to the neighbouring grid points. Also for the construction of the advection vector, two solutions are possible, also illustrated in Fig. 12. Either one can take the vector in point P, or the advection vector can "follow" the velocity field ("semi-Lagrangian"). In the further implementation of MAPLE, a semi-Lagrangian backward scheme was chosen. In the *right panel* of Fig. 12, the final results of the paper are presented: the lifetime of precipitation features for four different events. Experiments with a source-sink term were also carried out, but no consistent conclusions could be drawn from these tests.

In **Paper II** (Germann and Zawadzki, 2004), the deterministic point-forecast of paper I is converted into a *probability forecast*. Instead of predicting the reflectivity $Z(t_0 + \Delta t, \mathbf{x})$ (Z in dB at position $\mathbf{x}$, Δt the lead time) as was done in Paper I, here an expression is searched for the probability P that Z exceeds a certain threshold $\mathcal{L}$:

$$P(t_0 + \Delta t, \mathbf{x}, \mathcal{L}) = \text{Prob}\{Z(t_0 + \Delta t, \mathbf{x}) \geq \mathcal{L}\}$$

In Germann and Zawadzki (2004), different methods are explored to produce such probability forecasts; here we will only highlight the one that turned out to be the most reliable. This method, dubbed the "Local Lagrangian" probability forecast, determines the density distribution
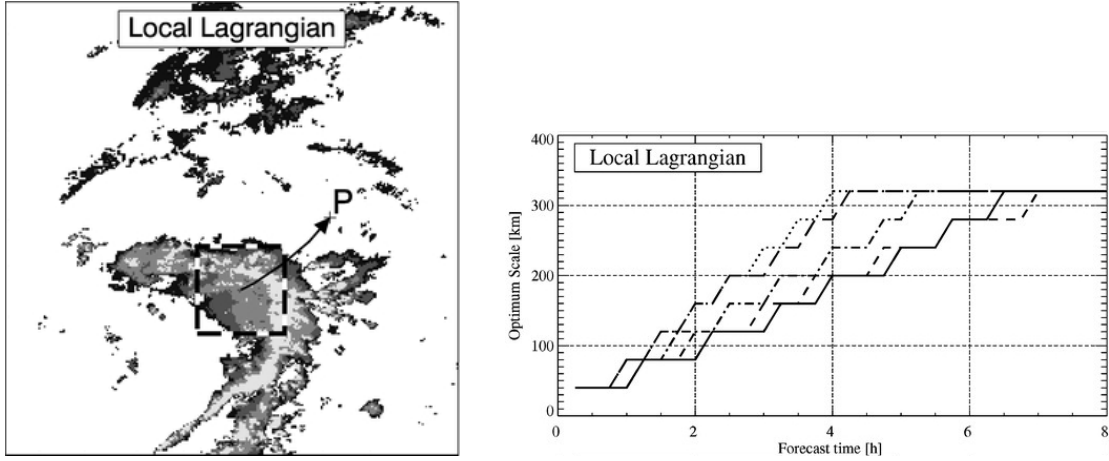
29

Figure 13: *Left panel*: Construction of the "Local Lagrangian" probability forecast. The dashed line shows the region selected to determine the probability distribution and P is the point of interest for which a forecast is issued. *Right panel*: Optimum scale (size of dashed box in left panel) in function of forecast lead time for five different cases. A step function is obtained, since only a discrete set of scales is considered here. The difference between the curves gives an idea of the case-to-case variability. Both figures from Germann and Zawadzki (2004).

of the parcel ω_k around O (in the terminology of Fig. 12), and applies this to construct a probability forecast for point P:

$$P(t_0 + \Delta t, \mathbf{x}, \mathcal{L}, k) = \text{Prob}\{Z(t_0 + \Delta t, \mathbf{x} - \boldsymbol{\alpha} + \mathbf{r}) \geq \mathcal{L} | \mathbf{x} + \mathbf{r} \in \omega_k\}$$

where $\mathbf{x} + \mathbf{r}$ is any arbitrary position within a square area ω_k of side length k, and $\boldsymbol{\alpha}$ is the advection vector from Fig. 12. The technique is illustrated in Fig. 13 (*left panel*). Since small scale features in the precipitation field have the shortest lifetimes (Paper I), the dimension of this area ω_k should depend on the lead time Δt. By studying the error score for a particular event, one can determine for each lead time the scale with the smallest error score, the "optimum scale". The optimum scale in function of forecast lead time is shown in Fig. 13 (*right panel*); the different curves are for four different events, and give an idea of the case-to-case variability of this optimum scale ω_k.

In **Paper III** of the series (Turner et al., 2004), the results of Paper I are taken as the motivation to construct a forecast filter that prevents small-scale precipitation patterns to be reproduced beyond their lifetime. The construction of such a filter is achieved by a spatial decomposition of the rainfield by means of a wavelet transformation. Wavelets are chosen for this purpose since they are less susceptible to the Gibbs effect (see Sect. 2.4) often present in an ordinary Fourier transform. In a wavelet transform (WT) the coefficients $W(m, x)$ for scale m and position x are calculated:

$$f(x) \xrightarrow{\text{WT}} W(m, x)$$

while the inverse wavelet transform reconstructs the original field, using a long-term weighted average $\overline{f(x)}$:

$$W(m, x), \overline{f(x)} \xrightarrow{\text{WT}^{-1}} f(x)$$

Now, the filtered forecast (I_{ff}) is obtained by multiplying the wavelet coefficients by weight functions $w(m)$ at each scale ($0 \leq w(m) \leq 1$):

$$w(m)W(m, x), \overline{f(x)} \xrightarrow{\text{WT}^{-1}} I_{\text{ff}}$$

These weights also depend on the lead time Δt. In an *a posteriori analysis*, the weights are constructed by correlating the different scales m of the semi-Lagrangian forecast (Paper I, Germann and Zawadzki, 2002), with the observed precipitation field. Scales with a low correlation are assigned small weights, which results in a lower rms error of the forecast. So in an a posteriori analysis, the "optimal forecast filter" (consisting of the set of $w(m, \Delta t)$ weighting functions) can be constructed. In an operational context, this is not possible of course, and a "near-optimal forecast filter" is constructed. This is done by comparing a forecast that was issued one hour ago with the present observation; the weights $w(m, 1h)$ can then be calculated. Assuming a relation between scale and lifetime, all weights are derived from the set $w(m, 1h)$, and a near optimal filter I_{nff} is constructed in this way. This filter can be used in a operational context.

There is, however, a drawback in the construction of spatial filters that wipe out the perishable scales with increasing lead time: the loss of information on the density distribution. The distribution of reflectivity or rainrate becomes more uniform with increasing forecast lead time, tending toward lower values. Therefore, some kind of rescaling is preferable, similar to the rescaling in S-PROG (see Sect. 4.11). Such a rescaling will improve the CSI score (taken at a certain moderate threshold, e.g. 15 dBZ), at the cost or the rms error. More on such a scaling will be given in Sect. 4.11.

Finally, **Paper IV** (Germann et al., 2006) focusses on the predictability of precipitation, starting from the results obtained in Paper I. We will not discuss this paper in detail, but only note here that one important result obtained by the authors is that the errors in a Lagrangian forecast due to the variability of the velocity field are small, but not negligible. This result nicely agrees with the findings of Bowler et al. (2006) (see STEPS, Sect. 4.13 and Fig. 15, *left panel*).

MAPLE is commercialised by the company "Weather Decision Technologies" at Oklahoma, U.S., a spin-off of the National Severe Storms Laboratory (NSSL) based in the same city. The algorithm is integrated in their "HydroMet Decision Support System" (HDSS, Conway and Eilts, 2004). The system is currently implemented in several places in the U.S. and abroad (northern Italy, Taiwan, Thailand).

4.9   NIMROD – U.K.

Main reference: Golding (1998)
For many years, NIMROD has been the "default" operational nowcasting system at the Met. Office in the U.K. Nimrod delivers routine predictions of rainfall rate, rain accumulation, precipitation type, snow probability, cloud cover, visibility and wind gust speeds. The precipitation forecast consists of two parts, an "advection part" of the forecast, and a NWP model forecast. Some of its features are already briefly discussed in Sect. 4.5 and 4.6. We also note here that in the NIMROD system, there is a real time hourly correction of the radar images with gauge accumulation data.

For the advection part, the rainfall field is first segmented into discrete, contiguous regions with a certain critical size, called *contiguous rain areas* (CRAs). Two different estimates are then made for the velocity vector of each CRA. The first one is the vector that maximises the correlation between the current position of the CRA and its position on a previous image (pattern matching). An alternative estimate is obtained by taking the NWP model wind field vector that realises the optimum correlation. The correlation measures are then used to make a final selection between the linear displacement and the model wind field, resulting in the "advection part" of the precipitation forecast.

The final precipitation forecast is compiled from a merging of this "advection part" with the NWP model forecast. In this final forecast, the weight of the advection forecast falls exponentially with forecast lead time. NIMROD's performance has been checked with the usual verification statistics, proving that NIMROD realises a substantial improvement over persistence

and NWP forecasts. NIMROD output is used to make the routine rainfall forecast for the U.K. available in real time on the Met. Office public website.

4.10 RadVil – France

Main reference: Boudevillain et al. (2006)
RadVil is a research system (not operational) developed in France by Boudevillain et al. (2006). The idea behind the system is not to advect rain rate or reflectivity as usual, but the *vertically integrated liquid* (VIL) water content (kg m^2) instead. The advection of VIL can be expressed in the formalism of Sect. 2:

$$\frac{d(\mathrm{VIL})}{dt} = S(t) - P(t) \quad \text{(advection equation)} \tag{5}$$

$$\text{with} \quad \frac{d(\cdot)}{dt} = u\frac{\partial}{\partial x} + v\frac{\partial}{\partial y} + \frac{\partial}{\partial t}$$

$S(t)$ source term

$P(t)$ precipitation

Eq. (5) can be understood easily: the water content will decrease if precipitation forms $(-P(t))$, and increase with a source term $(+S(t))$. The precipitation $P(t)$ is related to the VIL by the *response time* $\tau(t)$:

$$P(t) = \frac{\mathrm{VIL}(t)}{\tau(t)} \tag{6}$$

In this equation, both $P(t)$ and VIL(t) are known from a PCAPPI image resp. volume scan, and hence $\tau(t)$ can be calculated. The response time expresses the ability of the VIL water content to form precipitation. The source term $S(t)$ is estimated from two successive VIL fields in the past:

$$S(t) = \frac{\mathrm{VIL}(t) - \mathrm{VIL}^\star(t-\Delta t)}{\Delta t} + P(t)$$

where * denotes that the VIL field is advected before the subtraction. Using Eq. (6), Eq. (5) can now be written as

$$\frac{d(\mathrm{VIL})}{dt} + \frac{\mathrm{VIL}(t)}{\tau(t)} = S(t)$$

Integration leads to an estimate of the forecast VIL:

$$\mathrm{VIL}(t+dt) = \mathrm{VIL}^\star(t)e^{dt/\tau} - S(t)\tau(t)[1 - e^{dt/\tau}]$$

From this predicted VIL at $t + dt$, the precipitation is then derived using Eq. (6).

    The RadVil scheme has been tested on volume data of a single radar (Monte-Lema, MeteoSwiss) through a detailed case study of five events. The performance of RadVil was evaluated against classical advection and persistence, and it was concluded that RadVil performs significantly better in one event, and slightly better in the remaining four.

    Alternative versions were made, in which the VIL water content is calculated somewhat differently, taking into account the solid state of water above the 0° isotherm. Although these alternative versions are expected to be more realistic, the simplest version of RadVil seems to work best. The authors conclude, however, that the current version of RadVil is not (yet) suitable for practical applications. A weak point in the current version is that only one advection velocity is used for the whole domain.

4.11   S-PROG – Australia

Main reference: Seed (2003)

S-PROG is a spectral algorithm developed by dr. Alan W. Seed of the Bureau of Meteorology, Australia. The concept of a spectral approach is already explained in Sect. 2.4, and will not be repeated here. The basic idea is to decompose the reflectivity field (in dBZ) into a sum of k different levels (the "cascade"), with each level representing features of a particular scale, and to consider the evolution of these levels separately.

The evolution of the different levels is governed by an autoregressive (AR) scheme. An AR(2) scheme was chosen as the best compromise between complexity and calculation speed. In such a scheme, two Lagrangian correlation coefficients are calculated for each level k of the cascade, $\rho_{k,1}(t)$ and $\rho_{k,2}(t)$, by advecting respectively $Z_k(t-1)$ by $(\Delta x, \Delta y)$ and $Z_k(t-2)$ by $(2\Delta x, 2\Delta y)$. Note that the notation Z_k is used here, and not X_k as in Sect. 2.4, because we work here with the *normalised* levels. From the correlation coefficients $\rho_{k,1}(t)$ and $\rho_{k,2}(t)$, the AR(2) model parameters $\phi_{k,1}(t)$ and $\phi_{k,2}(t)$ are calculated by the Yule-Walker equations:

$$\phi_{k,1}(t) = \frac{\rho_{k,1}(t)\{\rho_{k,1}(t)[1 - \rho_{k,2}(t)]\}}{1 - \rho_{k,1}(t)^2}$$

$$\phi_{k,2}(t) = \frac{\rho_{k,2}(t) - \rho_{k,1}(t)^2}{1 - \rho_{k,1}(t)^2}$$

We have now all the elements to construct the forecast. The k levels $Z_{k,i,j}$ at time $t+1$ (at position i, j) are calculated

$$Z_{k,i,j}(t+1) = \phi_{k,1}(t)Z_{k,i,j}(t) + \phi_{k,2}(t)Z_{k,i,j}(t-1) \tag{7}$$

Then, iteratively, the k levels $Z_{k,i,j}$ at time $t+n+1$ are calculated

$$Z_{k,i,j}(t+n+1) = \phi_{k,1}(t)Z_{k,i,j}(t+n) + \phi_{k,2}(t)Z_{k,i,j}(t+n-1) \tag{8}$$

The levels Z_k in the right hand side of Eqs.(7) and (8) are obviously the fields advected by a multiples of $(\Delta x, \Delta y)$. The output forecast at position (i, j) is finally constructed by adding all the levels $Z_{k,i,j}$ for each time step.

The levels representing the smallest scales, normally have the lowest correlation values $\rho_{k,1}(t)$ and $\rho_{k,2}(t)$, since the smallest features in the rain field have on average the shortest lifetime. The low correlation values of the smallest scales ensure that the levels representing these scales fade out naturally. This is the strength of the spectral algorithm.

In the original version of S-PROG (Seed, 2003), the advection is done through a simple and robust area tracker, producing only one displacement vector for the whole field, and for all scales. This was acknowledged to be the major flaw in this first version of S-PROG. The advection was improved in a version of S-PROG implemented for a radar in the vicinity of Barcelona (Berenguer et al., 2005), discussed in the next section.

As was already briefly discussed for the MAPLE algorithm (Sect. 4.8), the removal of the smallest scales causes the distribution of reflectivity or rainrate to be more and more uniform with increasing forecast lead time. The rms error of a filtered forecast is improved, but the success rate (for a certain moderate or high threshold) will decrease. Therefore, filtered forecasts are often renormalised to correct for this power loss. In S-PROG, the forecast reflectivity field is renormalised in a way that the fraction of the field that exceeds a certain threshold (here 15 dBZ) is the same as in the original field. This is done as follows. First, the fraction f_{15} of the original field that exceeds 15 dBZ is calculated. Then, the threshold Z_f is searched that defines the same fraction in the forecast field. Since the forecast field is more uniform and is
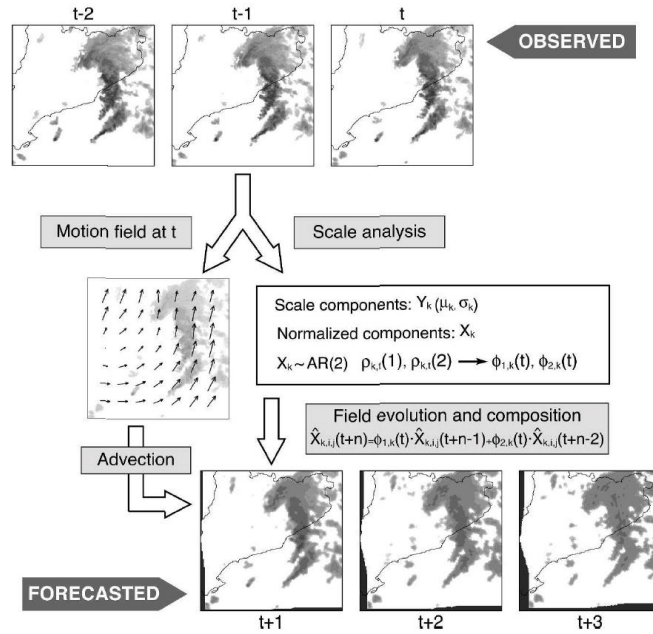
Figure 14: General scheme of the S-PROG algorithm as it has been implemented by Berenguer et al. (2005). The three latest scans (top of the figure) are used as input for both the velocity field analysis (middle left), and the spectral analysis (middle right). In this analysis, the field is decomposed and an autoregression (AR) analysis is performed on the different levels (see Sect. 4.11 for more details). The field is built up again, and advected with the calculated velocity field. Figure taken from Berenguer et al. (2005).

composed of lower values, this threshold Z_f will be lower than 15 dBZ. The forecast field is then normalised using

$$\mathrm{dBZ}_{i,j} = \begin{cases} \mathrm{dBZ}_{i,j} + (15 - Z_f) & \text{if dBZ}_{i,j} > Z_f \\ 0 & \text{otherwise.} \end{cases}$$

Of course, many other scaling methods could be implemented.

4.12   S-PROG – Spain

Main reference: Berenguer et al. (2005)
Berenguer et al. (2005) implemented a version of S-PROG (Seed, 2003) for the Barcelona area, in which the advection was improved. More specifically, the single displacement vector was replaced by a vector field derived by the COTREC method (Sect. 3.2). The general scheme of this method is given in Fig. 14.

Contrary to the original version of S-PROG (Seed, 2003), the performance of the current implementation has been studied by a detailed validation study. The validation was carried out from two different perspectives: (i) a direct verification in which the forecast radar fields are compared with the radar fields at verification time and (ii) a hydrological verification with hydrographs using a rainfall runoff model. Concerning (i), the S-PROG forecast is compared with an Eulerian and Lagrangian persistence forecast, the latter one using the same velocity field as S-PROG. The comparison indicates that S-PROG exhibits on average a higher skill than the two reference forecasts. From the hydrological point of view, S-PROG had no real advantage over the simpler methods. This is somehow expected, since a basin naturally averages out the small features, minimising the effect of the spatial filtering in S-PROG.

4.13   STEPS – U.K., Australia

Main reference: Bowler et al. (2006)

STEPS is, together with ANC (Sect. 4.2) one of the most advanced QPF systems currently available. It is developed at the Met. Office of the UK, in close collaboration with dr. Alan W. Seed of the BoM, Australia. A detailed description of the system can be found in the technical report of Bowler et al. (2004a). It is one of the few *probabilistic* QPF schemes. The system is a sophisticated combination of three elements: the spectral algorithm S-PROG (Sect. 4.11), an innovating noise injection into the forecast, and a downscaled NWP.

The concept of the whole system is the development of three different cascades. The first cascade, the "extrapolation cascade", is essentially the same cascade as in the S-PROG algorithm. The second cascade, the "noise cascade", is a cascade containing spatially and temporally correlated noise. Noise is injected into a specific scale if this scale looses skill in the forecast. Hence, the noise will be injected first into the smallest scales since the smallest rain features disappear first in the extrapolation cascade, while for the larger scales the noise injection will occur in a later time step. The noise cascade is driven by the same AR(2) model as the extrapolation cascade, and has the correct temporal correlation statistics. The third cascade is the downscaled NWP model, and ensures that the precipitation forecast evolves towards the large scale dynamical evolution of the atmosphere. Before the construction of the final forecast, the combination of the three cascades is realised for each level of the cascade separately, using weights that are derived from an estimate of the skill of that particular cascade.

The velocity field is constructed as a combination of a "diagnosed" velocity field and an NWP based velocity field. The diagnosed velocity field is calculated using optical flow, similar to the one in the GANDOLF+OF system (Sect. 4.6), except that here a backward-in-time advection scheme is used. Since OF can produce very noisy velocity fields in situations with fast moving cells, an overall advection vector for the whole field is applied before applying the OF scheme. Even then the velocity field is still quite noisy, and therefore a temporal smoothing is applied to the diagnosed field. The NWP field is not the wind field as e.g. in the Czech system (Sect. 4.4), but is derived in the same way as the diagnosed field: NWP precipitation forecasts are used in the OF analysis instead of radar images. The two velocity fields are then merged, using the same weights as in the cascade combination.

In Bowler et al. (2004a), also a study of the *advection errors* is presented. They show that the errors induced by the evolution of the velocity field are negligible compared to the errors induced by the evolution of the precipitation field (Fig. 15). This is in nice agreement with the recent results obtained by Germann et al. (2006). Even at lead times of 6 hours, advection errors account for only 10% of the total error in the forecast, indicating that the evolution of the precipitation itself is by far the most significant source of error. Based on this study of the advection errors, Bowler et al. (2004a) introduce a perturbation on the derived diagnosed velocity field. Special care is taken that the perturbed velocity field that is added to the diagnosed field has the appropriate statistical structure.

Since STEPS is a probabilistic forecast, the validation was done using the Brier skill score. The Brier skill score measures the improvement of a probabilistic forecast relative to a long-term climatology. The Brier skill score can take values from $-\infty$ to 1, where 1 is a perfect forecast, and 0 indicates no skill compared to climatology. The Brier skill score of STEPS is shown in Fig. 15 for different precipitation thresholds. It is shown that the skill of STEPS decreases with increasing lead time, and with increasing rain-rate threshold at which the verification is performed. The authors note that it is not possible to evaluate the skill of STEPS at higher rain rates (due to the very low probability of these high rain rates), unless a verification over a longer period is realised.

The strength of the system is that the system requires only a minimum of tuning. The
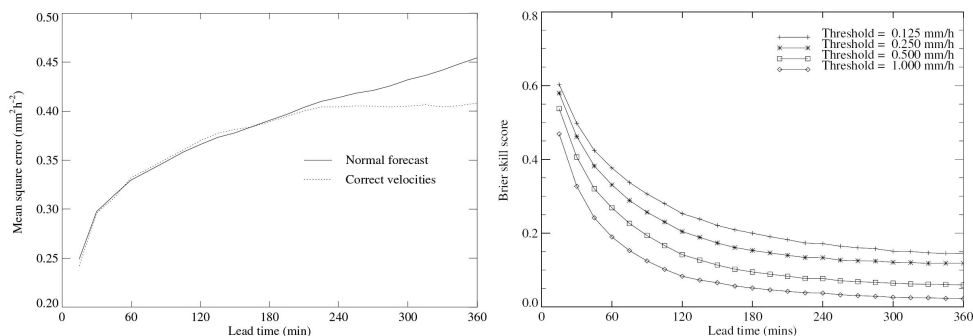
Figure 15: *Left panel*: The mean square error of the STEPS precipitation forecasts for lead times up to 6 hours. The full line ("Normal forecast") represents the forecast using a smooth velocity field that is derived at the issue time. The dotted line ("Correct velocities") represents the forecast using the correct velocities. Even at lead times of 6 hours, advection errors account for only 10% of the total error in the forecast. Similar results were obtained in Germann et al. (2006). *Right panel*: The Brier skill score of STEPS for different precipitation thresholds. Both figures taken from Bowler et al. (2006).

system is largely governed by the statistics produced during the analysis, completed by some tuning with climatological values. The core of STEPS is the S-PROG spectral algorithm. The critical assumption of this algorithm is that rainrates are log-normally distributed. Unfortunately, this is not always the case, e.g. in the passage of a frontal system, in which large areas of moderate rain prevail. STEPS tends to underestimate too little moderate rain in these cases. One should keep in mind that STEPS is also not tuned towards extreme events.

4.14   SWIRLS – Hong Kong

Main reference: Li and Lai (2004b)
SWIRLS (Short-range Warnings of Intense Rainstorms in Localized Systems) is a QPF system concentrating on heavy precipitation events. It is an advanced system combining an area tracker (an adapted version of TREC, Sect. 3.2) and a cell tracking algorithm (GTrack, similar to TITAN, Sect. 3.1). At the Hong Kong Observatory, SWIRLS is used in combination with an NWP component to extend the QPF to a time span of 24h ahead. More details on the operational aspects are given in Li and Lai (2004a). Here, we will limit our discussion to SWIRLS alone. One important innovation of SWIRLS is that it automatically adapts the Z-R relation in real time, as the rain event unfolds. Severe precipitation events often require a Z-R relation reflecting a drop-size distribution different from the widely used Marshall-Palmer relation. In this region, this is especially true during the monsoon season.

SWIRLS starts with the determination of the TREC vector field, with an optimised box size (Tuttle and Foote, 1990). The vector field is then filtered, and deviating vectors are replaced by the mean of the surrounding vectors. The noisy TREC field is turned into a realistic vector field. After the determination of the velocity field, the Z-R relation is adjusted in real time. This is done by comparing every five minutes the radar reflectivity with rain gauges underneath, using the CAPPI images of 1 km height. For every rain gauge, the corresponding pixel area on the CAPPI image is defined, and a least-squares fit is performed on the equation

$$\mathrm{dBZ} = 10 \log a + b \, \mathrm{dBG}$$

with dBG the rainfall measured by the rain gauges expressed in dB. Using the determined velocity field and the updated Z-R relation, the rain rate is advected. It should be noted, however,
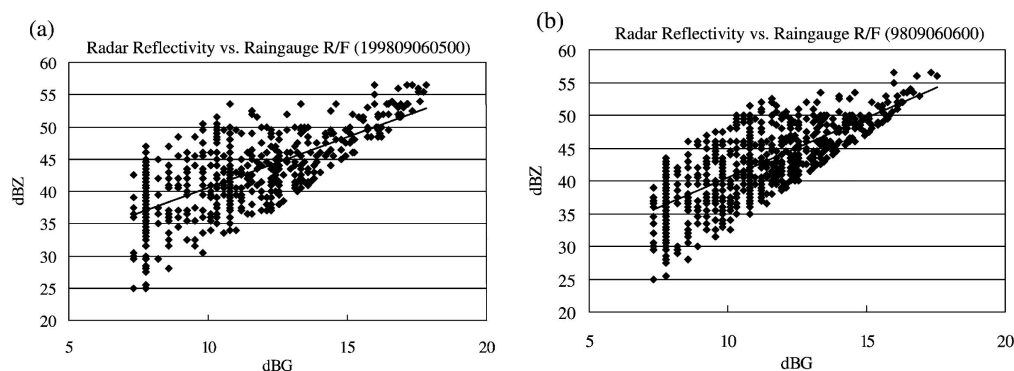
Figure 16: Two examples (one hour separated in time) of the determination of the Z-R relation by fit (solid line) through raingauge-radar pairs, as part of the SWIRLS system (Sect. 4.14). Figure taken from Li and Lai (2004b).

that a time step of five minutes for the gauge adjustment of the Z-R relation is extremely small: the noise on a five minute gauge measurement is expected to be quite high, and this will affect the accuracy of the Z-R relation considerably.

A well-known shortcoming of area trackers is that they are often unable to handle correctly situations in which storm cell movements differ from the larger storm volume movement. For these situations, SWIRLS also contains a centroid tracker. Similar to TITAN, the cell detection is defined by a fixed threshold, and a cell is represented by an ellipse. The cell tracking in GTrack is, however, not realised by a combinatorial cost function, but it is based on distance and size criteria. More precisely, the GTrack algorithm defines a searching radius for each individual cell, and an identification between parent and child is made if they have similar size. GTrack vectors that differ by more than 90° from the nearest TREC vectors, are removed.

Verification of SWIRLS is performed using the common validation measures (POD, FAR, CSI, Heidke skill score HSS), and indicates that SWIRLS is performing significantly better than a random forecast. SWIRLS definitely possesses some unique features, including the real-time adjustment of the Z-R relation. Another interesting feature is that it contains two different tracking algorithms, an area tracker and a cell tracker. For the moment, or at least in the version described in Li and Lai (2004b), these two vector fields coexist next to each other, but it would be better to combine the information to generate some kind of composite vector field. Future plans in the development of SWIRLS are the estimation of the echo decay and growth along the TREC vector field (Lagrangian evolution); the implementation of a perturbed SWIRLS QPF to realise an ensemble forecast; and the injection of additional data like satellite data and GPS moisture information.

4.15 TRT – Switzerland

Main reference: Hering et al. (2004)
The Thunderstorms Radar Tracking (TRT) system of MeteoSwiss is a nice example of a system that has evolved from a basic tracking tool to a more complete QPF system in recent years. The basic building block, the detection and tracking algorithm developed by Hering et al. (2004), was already described in detail in Sect. 3.1.5. Here we discuss the recent improvements implemented in TRT: the tracking procedure was improved by Hering et al. (2005); a more complete exploitation of the 3D data and a ingestion of other data into the system (e.g. lightning data) was realised by Hering et al. (2006).

It was realised that the cell velocities produced by the tracking algorithm as it was presented

in Hering et al. (2004) using area overlap, were not very accurate in cases of complex situations and splits/merges. The improved cell velocity calculation in Hering et al. (2005) consists of a combination of the overlap technique and a correlation technique similar to TREC. If the difference in cell area of two consecutive cells exceeds a certain threshold (default is 30%), then the velocity vector is no longer the connection of the gravity centers, but the vector is the translation realising the highest correlation between a reference window around the cell at the first volume scan, and a search window at the second scan (note some similarity with the CELLTRACK algorithm, Sect. 3.1.4).

The major improvement of the TRT system presented in Hering et al. (2006) is the improved exploitation of the 3D nature of the reflectivity scan. 2D cell-based attributes are calculated from the 3D volume scans, like cell-based VIL, echo tops and maximum reflectivity altitude. Cell-based VILs are calculated for each detected cell, and also the (cloud-to-ground) lightning data is ingested in the system. All these products are visualised in real-time for the end-user (forecaster) in a browser window (an integration in the NinJo visualisation system is planned in 2008; Hering et al., 2007).

Since TRT is built upon a cell tracker, it is optimised for severe convective events, and should obviously be used in these conditions only. MeteoSwiss started the diffusion of heavy thunderstorm warnings in the summer of 2005 in the form of simple news flashes on national and local radio stations. In this summer, 70 flashes were broadcast on a total of 18 warning days. The warnings are not automatically generated, but are edited by the forecasters. Nevertheless, forecasters acknowledged a substantial contribution of the TRT system to the flash-news. To rapidly alert the forecasters and focus their attention on the potentially most damaging cells, TRT was complemented with a new "cell severity ranking" product (Hering et al., 2008). This product displays only the most intense storms based on the computation of a single numerical parameter, removing all but the essential information. The identified cells are represented by a colour coded ellipse, and include also a 60 min position forecast which takes into account the uncertainty of the expected location of the cell.

4.16 Recent developments and experiments

In this section, we review very briefly some recent developments and experiments in the QPF field. The examples given below are intended to give only a flavour of the kind of research that is currently carried out in the broad context of QPF. This overview is certainly not meant to be exhaustive or complete.

4.16.1 Artificial Neural Networks (ANN) approach

The application of Artificial Neural Networks (ANN) in the domain of QPF has been the subject of several studies in the past (e.g. Grecu and Krajewski, 2000). Here, we briefly discuss a recent study by Chiang et al. (2007) made in Taiwan. Every neural network has a predefined *architecture* or *topology*, consisting of an input layer, a hidden or processing layer, and an output layer. To account for the dynamic nature of precipitation fields, an extra hidden layer is added, which acts as a kind of memory in the system: it stores relevant information of the previous time step(s). This system is classified as a "feedback network", contrary to feedforward neural networks in which the weights between the layers are stationary. An overview of the network topology that was used in Chiang et al. (2007) is given in Fig. 17. The general conclusion of the authors is that Artificial Neural Networks can be applied successfully in a QPF framework, leading to more reliable forecasts. However, ANNs can only be applied in situations similar as they were trained with. Since the network in the paper is trained with data of five typhoon
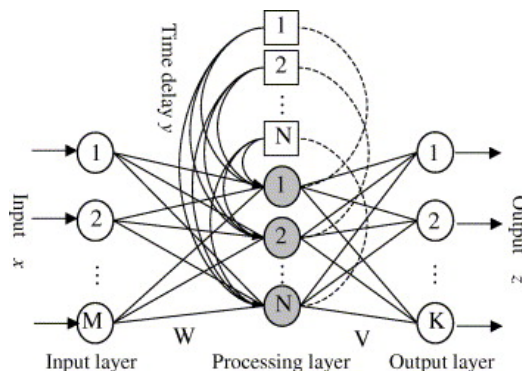
Figure 17: Topology of the Artificial Neural Network (ANN) used in Chiang et al. (2007). An extra layer (the upper part in the processing layer) is added to the usual ANN architecture, in order to account for the dynamic and time-varying character of precipitation.

events in the Taiwan area, the QPF system is not readily transferable to regions with different precipitation types.

4.16.2 Multiple regression models

Apart from ANN experiments, also the application of multiple (linear) regression methods in the QPF field is examined in the literature. In this section, we discuss the method recently developed by Sokol (2006) for the radar composite of the Czech Republic. A multiple regression method consists of a certain number (N) of *predictors* x_i and a number of predictands y_j. In a linear framework, a predictand y takes the form

$$y = a_0 + a_1 x_1 + \cdots + a_N x_N$$

where a_i are the model parameters. These model parameters are found by minimising the difference between the observed and the predicted values of y:

$$S = \sum_{i=1}^{n_c} (y_i - p_i)^2$$

where n_c is the number of predictands used in the minimisation. The number of predictors N has to be limited, and a selection of predictors containing the most information is necessary, eliminating as well predictors containing too much redundant information. The regression method has the tendency to underestimate heavy precipitation. To correct for this effect, a posterior correction is made on the model outputs p_i:

$$p_{\mathrm{cor},i} = \alpha\, p_i + \beta$$

with $\alpha > 1$. The parameters α and β are fitted using only the regions with the highest precipitation. The regression procedure together with the correction procedure is referred to as the REG forecast.

In this study, the predictors x_i are obtained from: (i) the radar precipitation field and derived fields (in 9×9 km squares); (ii) radar precipitation field advected by the 700 hPa wind fields derived from the NWP forecast ALADIN/LACE (advection forecast); and (iii) variables derived from ALADIN/LACE. The REG forecast is evaluated by comparing it to the advection forecast (note that this forecast is also included as a predictor field). The REG approach seems to produce

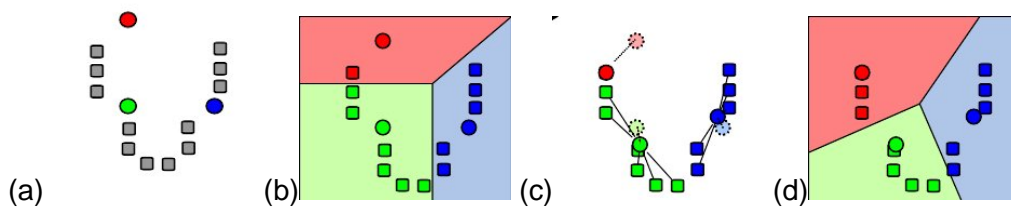(a)   (b)   (c)   (d)

Figure 18: Illustration of the K-Means clustering algorithm. In this basic example, only Euclidean distance is taken into account for the cluster definition. (a) In the first step, cluster center points are randomly distributed on the image; (b) pixels are grouped to the cluster for which their distance to the center point is minimal; (c) the centroids of the clusters are recalculated and taken as the new cluster centers; (d) steps b-c are repeated until the composition of the clusters does not change anymore.

on average better forecasts than the simple advection forecast. However, contrary to what was hoped for, REG did not succeed in forecasting the initiation and development of precipitation, which points to the fact that the predictors used in this scheme do not contain sufficient information for the prediction of precipitation evolution. This limits the forecast accuracy, especially in afternoon hours, when most of the storm initiation takes place. A possible solution suggested by the author is to include also other predictor fields, as e.g. satellite images.

4.16.3   K-Means clustering for segmentation

K-Means clustering is a segmentation technique that can be applied to any kind of image. The basic principle is shown in Fig. 18. In this simple example, the clustering is made only upon the geometrical distance. The K-Means clustering of pixels in a radar image is somewhat more complicated, since the value (and not only the position) of a pixel has to be taken into account as well. In the formulation of Lakshmanan et al. (2003), pixels are clustered on two opposing criteria:
• belong to the same cluster as your neighbours;
• belong to the cluster whose mean is closest to your value.
An example of a K-Means segmentation of a radar reflectivity image is shown in Fig. 19. After the segmentation, the motion field for the segments is estimated by moving a template of each segment around in the previous image. By comparing the average reflectivity value inside two matching templates, on can get also an estimate of the growth or decay. The motion of a specific pixel is obtained by a weighted combination of the motion of the nearby segments.

4.16.4   Kalman filter for smoothing

Lakshmanan et al. (2003) describes the application of the Kalman filter to a series of reflectivity images. The Kalman filter is a widely used mathematical tool nowadays, with numerous applications e.g. in computer graphics. It is in fact an estimator that is designed to cope with noisy measurements. A well known application of the Kalman filter is the estimation of the position of a missile, when only a limited number of noisy observations are available. For an introduction to the Kalman filter, we refer to the course notes of Welch and Bishop (2001). In Lakshmanan et al. (2003), the Kalman filter is used as a temporal smoothing tool for reflectivity images.
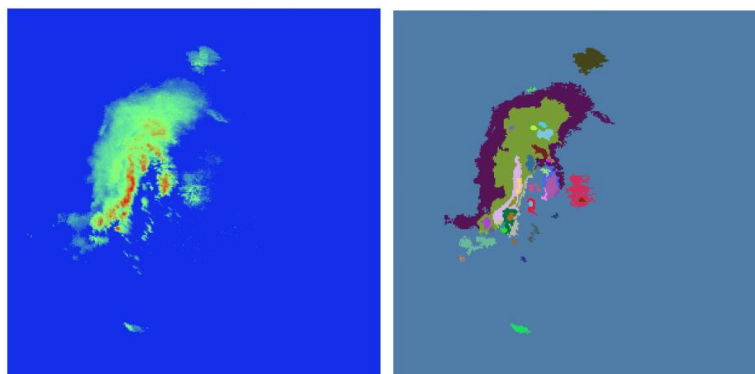
Figure 19: Example of a K-Means clustering of a radar reflectivity image. The original reflectivity image is shown on the left; the segmented image on the right. Figure taken from Lakshmanan et al. (2003).

4.16.5   WDSS-II

WDSS-II (Warning Decision Support System – Integrated Information) is "the second generation of a suite of algorithms and displays for severe weather analysis, warnings and forecasting". It is developed by the National Severe Storms Laboratory (NSSL) in cooperation with the University of Oklahoma. The homepage of the system is WWW.WDSSII.ORG, and it is described in detail in Lakshmanan et al. (2007). It is not only a collection of radar-related algorithms (e.g. algorithms for combination of scans, for hail diagnosis, etc. . .), but it contains also a programming environment (an application programming interface (API) library in C++) to develop new algorithms in this framework. Nice examples of products generated within the WDSS-II framework that are available for viewing in the Google Earth application, are given in Smith and Lakshmanan (2006).

4.17   Older or scarcely documented systems

Main reference: Mecklenburg et al. (2002).

2PiR   is the operational extrapolation QPF at Météo France. The velocity field is determined through a cross-correlation (area tracker) technique, with an additional filtering. Unfortunately, the system is not very well documented in the literature.

FRONTIERS   is the predecessor of NIMROD as the operational QPF system at Met. Office, U.K.

KONRAD   (KONvektionsentwicklung in RADarprodukten) is the extrapolation and nowcasting system of the Deutscher Wetterdienst (DWD, Germany).It uses a fixed threshold for cell detection, and concentrates its output in one summarising image.

PARAPLUIE   is a cell tracking and extrapolation algorithm described in Brémaud and Pointin (1993), developed at the University of Clermont-Ferrand, France. It is unclear whether this system is operational or not, and whether it is still maintained or further developed.

STNM   (Storm Tracker Nowcasting Model; Wolfson et al., 1999) is the storm tracker integrated in the WDSS system of the National Severe Storms Laboratory (NSSL) in the U.S. It is now largely replaced by the more recent SCIT algorithm (Sect. 3.1).

TIFS   (Thunderstorm Interactive Forecast System; Bally, 2004) is the operational nowcasting system for severe weather at the BoM (Australia). It bundles several systems discussed earlier in this paper (TITAN, SCIT, ANC, CARDS). TIFS is in fact a high-level interactive tool for forecasters, but it is also able to automatically generate warnings.

Univ. of Vienna   Steinacker et al. (2000) from the University of Vienna, Austria, developed a cell tracker which ingests, apart from radar reflectivity, also lightning density. Note that recently INCA is being developed as the operational QPF system at the Zentralanstalt für Meteorologie und Geodynamik (ZAMG) in Austria.

Other systems   (including HYRAD, SCOUT, SHARP and VSRF) are briefly discussed in Mecklenburg et al. (2002).

5   Towards a QPF at the RMI

5.1   General considerations

The development of any QPF system should start with a well-defined description of the user requirements. Before starting the actual development of a system, the developer should scrutinise the exact goals of the desired system. The following questions are therefore crucial, and should be discussed before starting the actual development:

Precipitation type   Should the desired system focus on *severe convection* with very high rain rates and related threats; or should the priority lie on a good extrapolation of *stratiform situations*, which are observed much more frequent than convective situations, although much less threatening? Of course, the ideal system is a system equally well performing in both situations, but it is inevitable that at a certain point choices will have to be made favouring either the prediction of large-scale complexes, or the extrapolation of individual cells. Some weather services have avoided this choice by developing a system consisting of a subsystem optimised for convective precipitation, and a subsystem optimised for stratiform situations.

Output   Should the QPF system produce a *deterministic* or a *probabilistic* forecast? End-users often prefer a deterministic precipitation forecast, but such a forecast only represents one of the many possible future situations, which is hopefully as close as possible to the real future situation. A probabilistic QPF, like e.g. MAPLE (Sect. 4.8, Germann and Zawadzki, 2004) or STEPS (Sect. 4.13, Bowler et al., 2006) is much harder to develop, but such a forecast is in fact a synthesis of all possible outcomes starting from the present initial conditions. Both types of forecast are in fact complementary.

Time base   The design of a QPF system is also determined by the required time span of the forecast. QPF systems producing forecasts for more than roughly 1 or 2 h ahead require input from NWP models. In convective situations, storm initiation and decay strongly limit simple extrapolation approaches. The time scale of the forecast is also connected to its spatial scale: in the previous section we have seen that continental scale QPFs (e.g. MAPLE, Sect. 4.8) are much longer valid than QPFs for smaller domains, but that their spatial resolution is much lower.

Users   Is the output of the QPF a tool that will be available to the *forecasters only*, or should the output be visible directly for the broad public, e.g. on the national weather service website and through derived products (SMS service, integration in car GPS systems, etc. . .). An intermediate (and most common) solution is a situation in which the output is exported only to the weather office and a limited number of selected clients, as for example the hydrological services or the civil protection authorities.

Warnings   Should the QPF system produce automated warnings in case of severe precipitation events, or should the forecaster on duty make these warnings? Note that any automatically generated warning should be verified by a human forecaster before its actual diffusion through the media.

5.2   Study of convective events in Belgium

The development of any QPF system for a certain area should be preceded by a climatological study of the precipitation of that area. For the development of a warning system, this study should mainly focus on convective storms: their frequency, typical lifecycle, growth and decay behaviour, preferred locations of initiation and trajectories.

Scientific research on severe convective storms on the Belgian territory is very limited. Forecaster Karim Hamid from the RMI published some detailed case studies of severe events in the latest decennium, in the form of internal RMI reports, or on a personal basis (see e.g. Hamid and Delobbe, 2007, more reports available upon request of the author K. Hamid). Every case study describes not only the convective event itself (with ample use of radar images), but also its broad meteorological context in which the event has developed, with satellite images, model outputs, soundings, and even damage reports. Radar images are discussed in detail, focusing on typical severe storm features like bow echoes and storm splitting. A recent climatological study of tornadoes and downburst in Belgium was published in an RMI report (Debontridder, 2008).

A *systematic* study of convective storms on Belgian territory is currently lacking. Very recently, our radar group started a 4-year research project to characterise the convective storm lifecycle. The main source of information for this study will be the radar archive of the RMI radar in Wideumont, operational since 2001, and the archive of the Belgocontrol radar in Zaventem, operational since 2003. The radar data will be complemented by data from the lightning detection system Safir, Meteosat images and derived products, tropospheric water vapour measurements by GPS, and NWP output (e.g. CAPE or CIN indices). The study should ultimately lead to a detailed knowledge of the tracks and lifecycle of convective events in Belgium, in relation to e.g. the initial mesoscale situation, the local orography, etc...This knowledge will form the basis of the future QPF system to be developed at the RMI.

The major task of this project will be a statistical study of the tracks of convective cells throughout the duration of a storm. Since tracking software is available in the literature, the first step should be the acquisition and installation of an existing storm cell tracker (see Sect. 2.3). TITAN is a relatively old algorithm, but it is widely used in the literature, it is free (for research usage) and open source. The weakness of the algorithm is that the cell detection is done through one fixed threshold. This limits the detection in the sense that a low threshold will detect too many cells, while a high threshold will miss emerging cells. More recent algorithms solve this issue by introducing an adaptive threshold, e.g. TRACE3D (Handwerker, 2002) and TRT (Hering et al., 2004, and successive papers). Therefore, we recommend the use of TITAN for a first exploration of the data, complemented by a more advanced algorithm in a later stage.

5.3   User requirements of an operational QPF

As discussed in Sect. 5.1, the design of a QPF strongly depends on the desired user requirements. In this section, we do a first attempt to evaluate the user requirements of both potential internal and external users of the QPF to be developed at the RMI.

5.3.1   Broad public

For the moment (Sept. 2008), the broad public has no free access to the RMI radar images in (near) real time. The only product available for the broad public on the RMI website www.meteo.be is an animation of the Belgian composite with a time resolution of 30 min and a minimum delay of 1 h. Paying customers receive the composite via the RMI service www.mymeteo.be, with a time resolution of 15 min and without delay. The same composite is offered (for free) on the website of the commercial weather forecasting company *MeteoServices*, with the same time resolution, but with a somewhat larger delay. The RMI radar images are also integrated in the commercial composite for Western-Europe *Meteox*, offering images in nearly real time with a time resolution of 15 min, complemented by an extrapolation for the next two hours. Unfortunately, no details are given on how this extrapolation is realised.
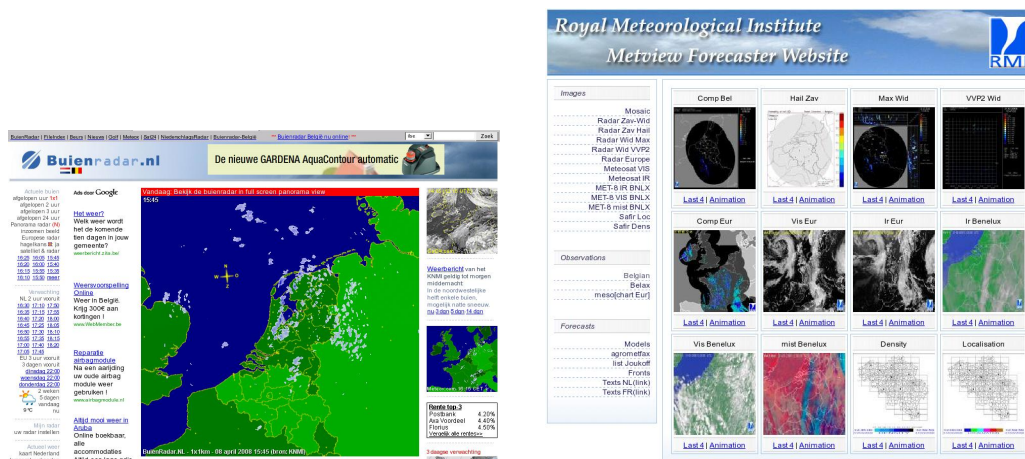
Figure 20: *Left panel*: snapshot of Buienradar.nl, the website of the private company Meteox that is responsible for commercialising the radar composite of the Dutch national weather service KNMI. It also offers an extrapolation of the rainrate for 2 hours ahead. The site is one of the most popular websites in the Netherlands. It has also a Belgian counterpart (buienradar.be), which is nothing more than the same composite, but limited to the Belgian territory. *Right panel*: main window (mosaic view) of the Metview Forecaster Website of the RMI (internal website). The future QPF system could be integrated into this website.

Although a dedicated scientific investigation in this matter is lacking, a large interest in radar data is certainly present amongst the broad public. Some national weather services sell their radar data to private companies, and these companies are then, in their turn, responsible for commercialising the images. The Dutch weather service KNMI has such an agreement with the private company Meteox that maintains the website WWW.BUIENRADAR.NL (Fig. 20, *left panel*), which is amongst the most popular websites in the Netherlands. Buienradar.nl offers a real-time radar animation of the radar composite (two radars) of the KNMI, with a time resolution of 5 min and an extrapolation of 2 hours ahead. The same composite and extrapolation is integrated in the Dutch traffic information site of the ANWB, as an overlay of the real-time traffic information map. The success of the website Buienradar.nl in the Netherlands (and also in Belgium) indicates a broad interest of the public in a detailed knowledge of rainfall, and its extrapolation for the next hour(s). A QPF designed for such a broad group of users, should be reliable in both convective and stratiform situations. On the other hand, a QPF developed for a hydrological service for example will have stricter quality demands than an on-line extrapolation tool for the broad public.

5.3.2 Weather office – extrapolation

In case of severe precipitation, forecasters are often expected to make precise predictions of when and where heavy rainfall will occur. Especially for these situations, forecasters are interested in a dedicated tool that facilitates the forecast task, but due to the complexity of such convective systems, precise predictions are almost impossible. A QPF that relies on cell tracking can, however, provide important information on the cells (e.g. tracks, age, evolution of certain characteristics like maximum reflectivity, echotop, VIL, etc. . .) that can be consulted on a graphical window. Forecasters working in weather services where such a tool is available (like TRT in Switzerland), generally appreciate the tool, and acknowledge that it can help in predicting the further evolution of a particular cell. Such a tool could be integrated as an additional
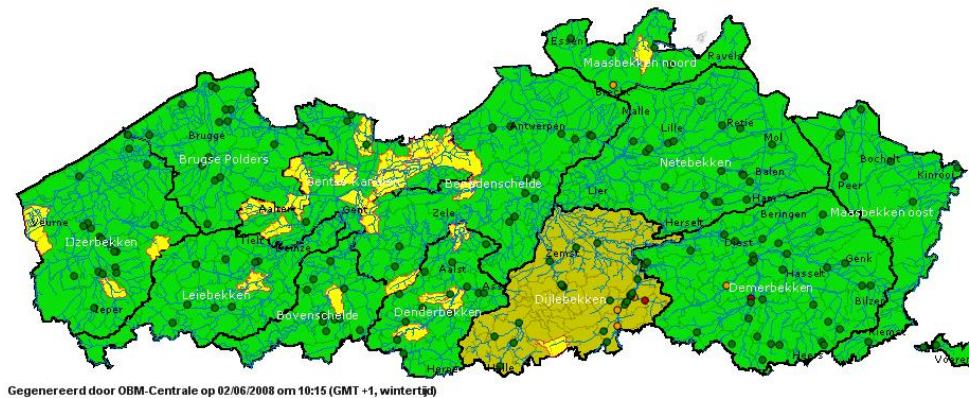
Figure 21:   Snapshot of the flood forecast system for the Flemish region on WWW.OVERSTROMINGSVOORSPELLER.BE, operated by the VMM. Flood warnings are issued for 48 hours ahead, taking the NIMROD extrapolation of the Belgian radar composite for the first 6 hours, and the precipitation prediction by the ALADIN NWP model for the time frame $6-48$h. The points are stage gauges that can be consulted in real time.

window in the internal Metview Forecaster Website (Fig. 20, *right panel*) of the RMI.

5.3.3   Weather office – warnings

For the moment, the RMI weather office issues short-term warnings for rain, iciness and snow, wind and thunderstorms. The warnings are issued on the RMI public website WWW.METEO.BE and they are integrated in EUMETNET's Meteoalarm project. The spatial resolution of the warnings is one warning per province ($\sim$3000 km^2). For the prediction of the initiation of severe weather, the RMI forecasters make use of several NWP output. On top of that, they are testing an in-house made checklist that consists of several parameters related to atmospheric instability, like KO-index, CAPE, etc. . . With this checklist, a score is calculated as a weighted sum of the different indices. This score is then a measure of the chance of the initiation of severe weather.

The type of warnings that will be produced based on an operational QPF, will be of a different kind than the warnings that are currently issued. The warnings for severe weather (which are, in this case, only warnings for heavy rain) will be more precise in location, but on a shorter time scale. Diffusion of the warnings to the public through the media should be as fast as possible. Since heavy rain has a serious impact on traffic safety, the diffusion of the warnings should preferentially be done through radio news flashes, and, in a later stage, through car GPS systems.

5.3.4   Hydrological requirements of the regions

Water management is a regional matter in the Belgian federal state. For the **Flemish region**, water management, waterways and hydrology are divided into several sections and agencies of the two departments "Leefmilieu, Natuur en energie" (Vlaamse Milieumaatschappij VMM) and "Mobiliteit en Openbare Werken" (Haven- en Waterbeleid, Waterbouwkundig Laboratorium, Waterwegen en Zeekanaal NV). The VMM operates an on-line flood forecast for the different Flemish basins: WWW.OVERSTROMINGSVOORSPELLER.BE; a snapshot of the flood forecast on this site is given in Fig. 21. Flood forecasts are made for the next 48 hours, taking radar data (Belgian composite, Fig. 2) as the primary input source for the hydrological model. More specifically, the NIMROD extrapolation is used for the first 6 hours, while the ALADIN NWP precipitation
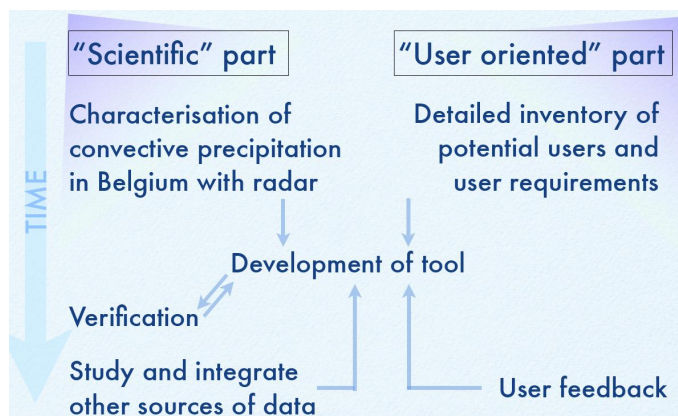
Figure 23: Roadmap for the QPF development at the RMI.

forecast is taken for more than 6 h ahead. The NIMROD system used by the VMM is an adapted version of the NIMROD system running at Met. Office in the U.K., discussed in Sect. 4.9.

In the **Walloon region**, waterways and hydrology are under supervision of the "Direction générale des Voies hydrauliques" of the "Ministère de l'Équipement et des Transports" (MET). Some catchments in this region that are very well covered by both the radar of Wideumont and rain gauges of the hydrological service (SETHY), have been studied in detail in several publications. The Ourthe catchment is studied in Berne et al. (2005) and Hazenberg et al. (2008) (a cooperation between the Wageningen University in the Netherlands, the MET and the RMI); the Ourthe and Semois in Leclercq et al. (2008) (a cooperation between the Université Catholique de Louvain (UCL), the MET and the RMI). The MET has its own real-time application for riverflow forecasting called HYDROMAX, developed at the UCL. This system is currently using rain gauges and water level chart recorders as input. In the future, also radar data will be ingested in this system. For this purpose, our group (Delobbe et al., 2008; Goudenhoofdt and Delobbe, 2008) is currently studying the optimal way for merging radar and rain gauge data for the Walloon region.

Interest for detailed precipitation forecasts for the **Brussels-Capital Region** is growing as well. Vulnerable points are identified at specific locations in the Brussels sewage network, tunnels and underground parking lots, and problematic zones on the Brussels territory are marked (see Fig. 22). An ambitious water management plan to prevent future floods is currently under study, and will be realised during the four coming years (IBGE/BIM, 2008a,b). In the context of this plan, the Brussels administration expressed their interest in a warning system for severe precipitation events for the different communes of the region.

5.4   Roadmap for the QPF development at RMI

In Fig. 23 a roadmap is sketched for the development of the future QPF tool at the RMI. It is a concise summary of this section. First, the development of the tool should be preceded by two different studies: one study
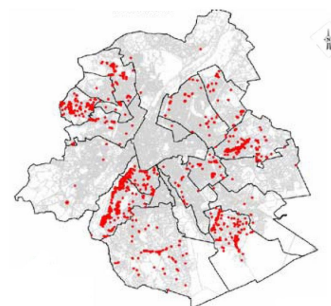

Figure 22: Localisation of flood claims by the inhabitants of the Brussels-Capital Region between 2003-2005. Figure taken from the report by IBGE/BIM (2008a,b)

dedicated to (convective) precipitation in Belgium using mainly radar observations, and another one dedicated to the requirements of the clients who will use the future QPF. Then, the actual development of the tool should start, with a strong emphasis on its verification. In a third stage, the tool should be extended with the ingestion of types of data other than radar. Simultaneously, from the user-side, the tool should be optimised following the users' feedback.

6   Conclusions

This document reviews the current status of Quantitative Precipitation Forecast (QPF) systems, operational ones and research systems, as a first step towards the development of an own QPF system at the Royal Meteorological Institute (RMI) of Belgium. The document consists of three main parts. In the *first part* (Sect. 2 and 3), we discussed the principles of QPF systems. We introduced Eulerian and Lagrangrian persistence, area and cell tracking, spectral approaches and expert systems. Several widely used tracking algorithms were discussed in more detail. In the *second part* (Sect. 4), a selection of operational and research QPF systems was discussed in more detail: their design, their usage, their strong and weak points. In the *third part* (Sect. 5) of this document, an overview is given of the possible requirements of potential internal and external users of a future QPF at the RMI.

A remarkable variety exists in the complexity of the existing QPF or nowcasting systems: some systems are built upon a simple tracker, while other systems ingest a variety of observations (ground and satellite) and pass them into sophisticated algorithms. It is often very difficult to prove the superiority of such an advanced system above a simple, transparent algorithm. The main reason is that the validation of a QPF is not obvious: rain complexes that are correctly forecast, but with a small deviation in place or time, can lead to very high error scores in some verification schemes. Ebert and McBride (2000) developed a verification procedure that takes this fact into account, and found that the location error is generally the dominant source of QPF error. Exciting new approaches for the verification of QPFs are currently under development: in Casati et al. (2004) a decomposition using Haar wavelets is used for this purpose. Several authors (e.g. Seed, 2008) note that QPF systems are well advanced nowadays, and that further improvements are unlikely to improve QPF significantly. Further development should therefore concentrate on the *prediction of the accuracy* instead of on the prediction itself.

Another important issue in the QPF development is the quality control of the radar data that is ingested into the QPF system. This topic was not covered by this document, since we chose to concentrate on QPF systems themselves, and not on the input data. Nevertheless, poor quality can destroy a good algorithm, so one should always be aware of what radar data quality is assumed by the QPF schemes. Examples are known of algorithms that performed very well in one environment, while they failed in another. Also, will a method derived from a state-of-the-art research radar also perform well on operational radars? We did not focus on these issues in this paper, but it is clear that the answers on these questions are very important for the final success of any QPF.

The actual development of an operational QPF at the RMI should be preceded by two dedicated studies. The first one is a detailed systematic study of convective precipitation in Belgium, primarily based on radar images, complemented by other sources (e.g. satellite products, GPS water vapour, lightning detection, etc. . .). This study will contribute to a better understanding of the initiation and evolution of convection over Belgium, and will provide important clues for the design of the future QPF system. A second study is a detailed overview of the requirements that the system should have, requirements provided by the potential future users (forecasters, hydrological services, civil protection authorities, broad public, etc. . .). Sect. 5.3 is a first step of such an overview, but still a lot of clarification is needed here. The design of the future QPF should ultimately rely on both the results of the characterisation of the convective precipitation events, and a detailed formulation of the user requirements.

List of acronyms

ALADIN   Aire Limitée Adaptation dynamique Développement InterNational
NWP model by a consortium of 16 (Sept. 2008) European partners

AMV   Atmospheric Motion Vectors
EUMETSAT algorithm for motion detection on satellite images

ANC   Auto Nowcast system
nowcasting system of NCAR, see Sect. 4.2

ANN   Artificial Neural Network
mathematical model based on biological neural networks

BoM   Bureau of Meteorology
national weather service of Australia

CAPE   Convective Available Potential Energy
measure of the unstability of the atmosphere, derived from a sounding

CAPPI   Constant Altitude Plan Position Indicator
horizontal cross-section of radar data at constant altitude

CARDS   Canadian Radar Decision Support
nowcasting system of national weather service in Canada, see Sect. 4.3

CHMI   Czech Hydrometeorological Institute
national weather service of the Czech Republic

CIN   Convective Inhibition
amount of energy needed to initiate convection

COTREC   COntinuity of TREC vectors
area tracking algorithm, see Sect. 2.2

CRA   Contiguous Rain Area
precipitating area in the NIMROD terminology

CSI   Critical Success Index
verification statistic, see note below

DWD   Deutscher Wetterdienst
national weather service of Germany

ECMWF   European Centre for Medium-Range Weather Forecasts
international organisation (31 members) based at Reading, U.K.

FAR   False Alarm Ratio
verification statistic, see note below

HSS   Heidke skill score
verification statistic, see note below

INCA   Integrated Nowcasting through Comprehensive Analysis
nowcasting system of weather service of Austria, see Sect. 4.7

KNMI   Koninklijk Nederlands Meteorologisch Instituut
national weather service of The Netherlands

MAPLE   McGill Algorithm for Precipitation Nowcasting Using Semi-Lagrangian Extrapolation
QPF algorithm by the radar group of the McGill university, Canada, see Sect. 4.8

NCAR   National Center for Atmospheric Research
non-governmental research institute in the U.S.

NOAA   National Oceanic and Atmospheric Administration
federal scientific agency in the U.S. for oceans and atmosphere

NSSL   National Severe Storms Laboratory
NOAA research laboratory for severe weather, in Oklahoma, U.S.

NWP   Numerical Weather Prediction

mathematical model of the atmosphere for weather prediction

OF   Optical Flow

implementation of Lagrangian persistence, see Sect. 2.1

OFC   Optical Flow Constraint

additional equation to solve OF

OOM   Object Oriented Model

programming method in which not functions, but objects are central

OPERA   Operational Programme for the Exchange of weather RAdar information

European radar network supported by EUMETNET

POD   Probability Of Detection

verification statistic, see note below

QPF   Quantitative Precipitation Forecast

precipitation prediction for short ($<$ 6h) lead times

RMI   Royal Meteorological Institute

national weather service of Belgium

SCIT   Storm Cell Identification and Tracking

cell tracking algorithm, see Sect. 3.1.2

S-PROG   Spectral Prognosis

spectral algorithm for QPF, see Sect. 4.11

STEPS   Short-Term Ensemble Prediction System

probabilistic QPF largely bases on S-PROG, see Sect. 4.13

STNM   Storm Tracker Nowcasting Model

cell tracking algorithm, see Sect. 4.17

SWIRLS   Short-range Warning of Intense Rainstorms in Localized Systems

QPF system in Hong Kong, see Sect. 4.14

TITAN   Thunderstorm Identification Tracking Analysis and Nowcasting

cell tracking algorithm, see Sect. 3.1.1

TREC   Tracking Radar Echo by Correlations

area tracking algorithm, see Sect. 2.2

TRT   Thunderstorms Radar Tracking

cell tracking algorithm, see Sect. 3.1.5

VET   Variational Echo Tracking

area tracking algorithm used in MAPLE, see Sect. 3.2.2

VIL   Vertically Integrated Liquid

estimate of total mass of precipitation in the clouds

VMM   Vlaamse Milieumaatschappij

Regional governmental body responsable for environment in Flanders

WDSS-II   Warning Decision Support System – Integrated Information

collection of QPF algorithms and programming environment, from NSSL

WSR-88D Weather Surveillance Radar, 1988, Doppler

NOAA's network of 158 (Sept. 2008) Doppler weather radars in the U.S.

ZAMG   Zentralanstalt für Meteorologie und Geodynamik

national weather service of Austria

A short note on

Verification statistics

A "binary" forecast (whether an event will happen or not) is often verified using a "contingency table" that shows the frequency of "yes" and "no" forecasts and occurrences. Hence, a contingency table contains the following elements:

		Observed	
		yes	no
Forecast	yes	hits	false alarms
	no	misses	correct negatives

Several verification statistics can be calculated with such a table, e.g.

$$\text{POD} \quad = \quad \text{probability of detection} \quad = \quad \frac{\text{hits}}{\text{hits} + \text{misses}}$$

$$\text{FAR} \quad = \quad \text{false alarm ratio} \quad = \quad \frac{\text{false alarms}}{\text{hits} + \text{false alarms}}$$

$$\text{CSI} \quad = \quad \text{critical success index} \quad = \quad \frac{\text{hits}}{\text{hits} + \text{misses} + \text{false alarms}}$$

An example of a more advanced score is the Heidke skill score (HSS):

$$\text{HSS} \quad = \quad \frac{(\text{hits + correct negatives}) - (\text{expected correct})_{\text{random}}}{N - (\text{expected correct})_{\text{random}}}$$

where

$$(\text{expected correct})_{\text{random}} = \frac{1}{N} \left[\begin{array}{l} (\text{hits + misses})(\text{hits + false alarms}) + (\text{correct negatives +} \\ \text{misses})(\text{correct negatives + false alarm}) \end{array} \right]$$

and N = (hits + misses + false alarms + correct negatives). The Heidke skill score measures the fraction of correct forecasts after eliminating those forecasts which would be correct due purely to random chance.

For more information on these statistics, see e.g. the extensive website of dr. Elizabeth E. Ebert (BoM, Australia) on forecast verification "Forecast Verification – Issues, Methods and FAQ" on HTTP://WWW.BOM.GOV.AU/BMRC/WEFOR/STAFF/EEE/VERIF/VERIF_WEB_PAGE.HTML. A standard text book for forecast verification is "Forecast Verification: A Practitioner's Guide in Atmospheric Science" (Jolliffe and Stephenson, 2003).

Acknowledgements

References

Auer, M., A. Jann, and A. Wirth, 2007: GaliMet – application of satellite-based location services for warnings against hazardous weather (an ARTIST III project). *ZAMG internal report*.

Austin, G. L. and A. Bellon, 1974: The use of digital weather radar records for short-term precipitation forecasting. *Quarterly Journal of the Royal Meteorological Society*, **100**, 658–664.

Bally, J., 2004: The Thunderstorm Interactive Forecast System: turning automated thunderstorm tracks into severe weather warnings. *Weather and Forecasting*, **19**, 64–72.

Bellon, A. and G. L. Austin, 1978: The evaluation of two years of real-time operation of a short-term precipitation forecasting procedure (SHARP). *Journal of Applied Meteorology*, **17**, 1778–1787.

Berenguer, M., C. Corral, R. Sánchez-Diezma, and D. Sempere-Torres, 2005: Hydrological validation of a radar-based nowcasting technique. *Journal of Hydrometeorology*, **6**, 532–549.

Berne, A., M. ten Heggeler, R. Uijlenhoet, L. Delobbe, P. Dierickx, and M. de Wit, 2005: A preliminary investigation of radar rainfall estimation in the Ardennes region and a first hydrological application for the Ourthe catchment. *Natural Hazards and Earth System Science*, **5**, 267–274.

Boudevillain, B., H. Andrieu, and N. Chaumerliac, 2006: Evaluation of RadVil, a radar-based very short-term rainfall forecasting model. *Journal of Hydrometeorology*, **7**, 178–189.

Bowler, N., C. Pierce, and A. Seed, 2004a: Steps: A probabilistic precipitation forecasting system which merges an extrapolation nowcast with downscaled NWP. *Met Office Forecasting Research Tech. Report*, No. 433.

Bowler, N. E., C. E. Pierce, and A. W. Seed, 2006: STEPS: A probabilistic precipitation forecasting scheme which merges an extrapolation nowcast with downscaled NWP. *Quarterly Journal of the Royal Meteorological Society*, **132**, 2127–2155.

Bowler, N. E. H., C. E. Pierce, and A. Seed, 2004b: Development of a precipitation nowcasting algorithm based upon optical flow techniques. *Journal of Hydrology*, **288**, 74–91.

Brémaud, P. J. and Y. B. Pointin, 1993: Forecasting heavy rainfall from rain cell motion using radar data. *Journal of Hydrology*, **142**, 373–389.

Casati, B., G. Ross, and D. B. Stephenson, 2004: A new intensity-scale approach for the verification of spatial precipitation forecasts. *Meteorological Applications*, **11**, 141–154.

Chiang, Y.-M., F.-J. Chang, B. J.-D. Jou, and P.-F. Lin, 2007: Dynamic ANN for precipitation estimation and forecasting from radar observations. *Journal of Hydrology*, **334**, 250–261.

Conway, J. and M. D. Eilts, 2004: The hydromet decision support system: new applications in hydrology. *Proceedings of the Third European Conference on Radar Meteorology (ERAD), Visby, Sweden, 6 - 10 September 2004*, 525–527.

Debontridder, L., 2008: Enkele klimatologische aspecten van tornado's, downbursts en hun schadeclassificaties. *Internal RMI report*.

Delobbe, L., G. Bastin, P. Dierickx, E. Goudenhoofdt, G. Leclercq, L. Moens, and M. Thunus, 2008: Evaluation of several radar-gauge merging techniques for operational use in the Walloon region of Belgium. *Proceedings of the International Symposium on Weather Radar and Hydrology, Grenoble, France, 10 - 15 March 2008.*

Delobbe, L. and I. Holleman, 2006: Uncertainties in radar echo top heights used for hail detection. *Meteorological Applications*, **13**, 361–374.

Dixon, M. and G. Wiener, 1993: TITAN: Thunderstorm identification, tracking, analysis, and nowcasting – a radar-based methodology. *Journal of Atmospheric and Oceanic Technology*, **10**, 785–797.

Doviak, R. J. and D. S. Zrnić, 1993: *Doppler Radar and Weather Observations*. Academic Press, 2nd edition.

Ebert, E. E. and J. L. McBride, 2000: Verification of precipitation in weather systems: determination of systematic errors. *Journal of Hydrology*, **239**, 179–202.

Germann, U. and I. Zawadzki, 2002: Scale-dependence of the predictability of precipitation from continental radar images. Part I: Description of the methodology. *Monthly Weather Review*, **130**, 2859–2873.

Germann, U. and I. Zawadzki, 2004: Scale dependence of the predictability of precipitation from continental radar images. Part II: Probability forecasts. *Journal of Applied Meteorology*, **43**, 74–89.

Germann, U., I. Zawadzki, and B. Turner, 2006: Predictability of precipitation from continental radar images. Part IV: Limits to prediction. *Journal of the Atmospheric Sciences*, **63**, 2092–2108.

Golding, B. W., 1998: NIMROD: A system for generating automated very short range forecasts. *Meteorological Applications*, **5**, 1–16.

Goudenhoofdt, E. and L. Delobbe, 2008: Evaluation of radar-gauge merging methods for quantitative precipitation estimates. *Hydrology and Earth System Sciences*, submitted.

Grecu, M. and W. F. Krajewski, 2000: A large-sample investigation of statistical procedures for radar-based short-term quantitative precipitation forecasting. *Journal of Hydrology*, **239**, 69–84.

Haiden, T., A. Kann, G. Pistotnik, K. Stadlbacher, M. Steinheimer, F. Wimmer, and C. Wittmann, 2006: Integrated Nowcasting through Comprehensive Analysis (INCA) - system overview. *ZAMG internal report, version 27 January 2006*.

Hamid, K. and L. Delobbe, 2007: F3-tornado in Belgium. *Proceedings of the 4th European Conference on Severe Storms, Trieste, Italy, 10 - 14 September 2007*.

Hand, W. H. and B. J. Conway, 1995: An object-oriented approach to nowcasting showers. *Weather and Forecasting*, **10**, 327–341.

Handwerker, J., 2002: Cell tracking with TRACE3D - a new algorithm. *Atmospheric Research*, **61**, 15–34.

Hazenberg, P., H. Leijnse, R. Uijlenhoet, and L. Delobbe, 2008: Hydrological modeling of the Ourthe catchment using both radar and raingauge data. *Proceedings of the International Symposium on Weather Radar and Hydrology, Grenoble, France, 10 - 15 March 2008*.

Hering, A. M., P. Ambrosetti, U. Germann, and S. Sénési, 2007: Operational nowcasting of thunderstorms in the Alpine area. *Proceedings of the 4th European Conference on Severe Storms, Trieste, Italy, 10 - 14 September 2007*.

Hering, A. M., U. Germann, M. Boscacci, , and S. Sénési, 2008: Operational nowcasting of thunderstorms in the Alps during MAP D-PHASE. *Proceedings of the Fifth European Conference on Radar Meteorology (ERAD), Helsinki, Finland, 30 June - 4 July 2008*.

Hering, A. M., U. Germann, M. Boscacci, and S. Sénési, 2006: Operational thunderstorm nowcasting in the Alpine region using 3D-radar severe weather parameters and lightning data. *Proceedings of the Fourth European Conference on Radar Meteorology (ERAD), Barcelona, Spain, 18 - 22 September 2006*, 453–456.

Hering, A. M., C. Morel, G. Galli, S. Sénési, P. Ambrosetti, and M. Boscacci, 2004: Nowcasting thunderstorms in the Alpine region using a radar based adaptive thresholding scheme. *Proceedings of the Third European Conference on Radar Meteorology (ERAD), Visby, Sweden, 6 - 10 September 2004*, 206–211.

Hering, A. M., S. Sénési, P. Ambrosetti, and I. Bernard-Bouissières, 2005: Nowcasting thunderstorms in complex cases using radar data. *Proceedings of The World Weather Research Programme Symposium on Nowcasting and very short Range Forecasting (WSN05), Toulouse, France, 5 - 9 September 2005*.

Hilst, G. R. and J. A. Russo, 1960: An objective extrapolation technique for semiconservative fields with an application to radar patterns. *Tech. Memo. No. 3, Travelers Weather Research Center, Hartford, CT*.

Hohti, H., J. Koistinen, P. Nurmi, E. Saltikoff, and K. Holmlund, 2000: Precipitation nowcasting using radar-derived atmospheric motion vectors. *Physics and Chemistry of the Earth, Part B: Hydrology, Oceans and Atmosphere*, **25**, 1323–1327.

Holleman, I., L. Delobbe, and A. Zgonc, 2008: The European weather radar network (OPERA): An opportunity for hydrology! *Proceedings of the International Symposium on Weather Radar and Hydrology, Grenoble, France, 10 - 15 March 2008*.

IBGE/BIM, 2008a: Gewestelijk plan voor overstromingsbestrijding - voorontwerp van regenplan 2008-2011. *Leefmilieu Brussel - BIM,* HTTP://DOCUMENTATIE.LEEFMILIEUBRUSSEL.BE/.

IBGE/BIM, 2008b: Plan régional de lutte contre les inondations - projet de plan pluie 2008-2011. *Bruxelles Environnement - IBGE,* HTTP://DOCUMENTATION.BRUXELLESENVIRONNEMENT.BE/.

Joe, P., L. Liping, W. Hongyan, J. Wilson, R. Roberts, and A. Seed, 2008: Assessing the quality of the radar data for the B08 forecast demonstration project. *Proceedings of the Fifth European Conference on Radar Meteorology (ERAD), Helsinki, Finland, 30 June - 4 July 2008*.

Johnson, J. T., P. L. MacKeen, A. Witt, E. D. Mitchell, G. J. Stumpf, M. D. Eilts, and K. W. Thomas, 1998: The Storm Cell Identification and Tracking algorithm: An enhanced WSR-88D algorithm. *Weather and Forecasting*, **13**, 263–276.

Jolliffe, I. T. and D. B. Stephenson, (Eds.) , 2003: *Forecast Verification: A Practitioner's Guide in Atmospheric Science*. John Wiley and Sons.

Kyznarová, H. and P. Novák, 2005: Development of cell-tracking algorithm in the czech hydrometeorological institute. *Proceedings of The World Weather Research Programme Symposium on Nowcasting and very short Range Forecasting (WSN05), Toulouse, France, 5 - 9 September 2005.*

Kyznarová, H. and P. Novák, 2007: CELLTRACK - convective cell tracking algorithm and its use for deriving of life cycle characteristics. *Proceedings of the 4th European Conference on Severe Storms, Trieste, Italy, 10 - 14 September 2007.*

Lakshmanan, V., R. Rabin, and V. DeBrunner, 2003: Multiscale storm identification and forecast. *Atmospheric Research*, **67-68**, 367–380.

Lakshmanan, V., T. Smith, G. Stumpf, and K. Hondl, 2007: The Warning Decision Support System – Integrated Information. *Weather and Forecasting*, **22**, 596–612.

Laroche, S. and I. Zawadzki, 1994: A variational analysis method for retrieval of three-dimensional wind field from single-doppler radar data. *Journal of the Atmospheric Sciences*, **51**, 2664–2682.

Leclercq, G., G. Bastin, L. Moens, L. Delobbe, P. Dierickx, and M. Thunus, 2008: Using weather radar measurements for real-time river flow forecasting. *Proceedings of the International Symposium on Weather Radar and Hydrology, Grenoble, France, 10 - 15 March 2008.*

Li, L., W. Schmid, and J. Joss, 1995: Nowcasting of motion and growth of precipitation with radar over a complex orography. *Journal of Applied Meteorology*, **34**, 1286–1300.

Li, P. W. and E. S. Lai, 2004a: Applications of radar-based nowcasting techniques for mesoscale weather forecasting in Hong Kong. *Meteorological Applications*, **11**, 253–264.

Li, P. W. and E. S. T. Lai, 2004b: Short-range quantitative precipitation forecasting in Hong Kong. *Journal of Hydrology*, **288**, 189–209.

Mecklenburg, S., J. Joss, and W. Schmid, 2000: Improving the nowcasting of precipitation in an Alpine region with an enhanced radar echo tracking algorithm. *Journal of Hydrology*, **239**, 46–68.

Mecklenburg, S., A. Jurczyk, J. Szturc, , and K. Ośródka, 2002: Quantitative precipitation forecasts (QPF) based on radar data for hydrological models. *COST Action 717: Use of radar observations in hydrological and NWP models.*

Mueller, C., T. Saxen, R. Roberts, J. Wilson, T. Betancourt, S. Dettling, N. Oien, and J. Yee, 2003: NCAR Auto-Nowcast System. *Weather and Forecasting*, **18**, 545–561.

Novák, P., 2007: The Czech Hydrometeorological Institute's severe storm nowcasting system. *Atmospheric Research*, **83**, 450–457.

Novák, P., L. Březková, P. Frolík, and H. Kyznarová, 2008: Use of radar-based quantitative precipitation forecast in hydrological modeling. *Proceedings of the Fifth European Conference on Radar Meteorology (ERAD), Helsinki, Finland, 30 June - 4 July 2008.*

Novák, P. and H. Kyznarová, 2006: Cell-oriented forecasts of czech weather radar data. *Proceedings of the Fourth European Conference on Radar Meteorology (ERAD), Barcelona, Spain, 18 - 22 September 2006*, 453–456.

Peura, M. and H. Hohti, 2004: Optical flow in radar images. *Proceedings of the Third European Conference on Radar Meteorology (ERAD), Visby, Sweden, 6 - 10 September 2004*, 454–458.

Peura, M. and H. Hohti, 2005: Motion vectors in weather radar images. *Proceedings of the 7th International Winds Workshop, Helsinki, Finland, 14 - 17 June 2004*.

Pierce, C. E., P. J. Hardaker, C. G. Collier, and C. M. Haggett, 2000: GANDOLF: a system for generating automated nowcasts of convective precipitation. *Meteorological Applications*, **7**, 341–360.

Pierce, C. E., et al., 2004: The nowcasting of precipitation during sydney 2000: An appraisal of the QPF algorithms. *Weather and Forecasting*, **19**, 7–21.

Rinehart, R. E., 2004: *Radar for Meteorologists*. Rinehart Publications, 4th edition.

Rinehart, R. E. and E. T. Garvey, 1978: Three-dimensional storm motion detection by conventional weather radar. *Nature*, **273**, 287–289.

Schmid, W., A. Mathis, and U. Keller, 2002: Nowcasting the risk of snowfall and freezing rain with radar and ground data. *New Challenges for Winter Road Service. XIth International Winter Road Congress, Sapporo, Japan, 28 - 31 January 2002*.

Schmid, W., S. Mecklenburg, and J. Joss, 2000: Short-term risk forecasts of severe weather. *Physics and Chemistry of the Earth, Part B: Hydrology, Oceans and Atmosphere*, **25**, 1335–1338.

Schmid, W. and M. Wüest, 2005: Verifying warnings for point precipitation. *Atmospheric Research*, **77**, 347–353.

Seed, A. W., 2003: A dynamic and spatial scaling approach to advection forecasting. *Journal of Applied Meteorology*, **42**, 381–388.

Seed, A. W., 2008: Quantitative precipitation forecasting: a review. *Proceedings of the International Symposium on Weather Radar and Hydrology, Grenoble, France, 10 - 15 March 2008*.

Smith, T. M. and V. Lakshmanan, 2006: Utilizing Google Earth as a GIS platform for weather applications. *22nd International Conference on Interactive Information Processing Systems for Meteorology, Oceanography, and Hydrology, Atlanta, GA, 29 January - 2 February 2006*.

Sokol, Z., 2006: Nowcasting of 1-h precipitation using radar and NWP data. *Journal of Hydrology*, **328**, 200–211.

Steinacker, R., M. Dorninger, F. Wölfelmaier, and T. Krennert, 2000: Automatic tracking of convective cells and cell complexes from lightning and radar data. *Meteorology and Atmospheric Physics*, **72**, 101–110.

Turner, B. J., I. Zawadzki, and U. Germann, 2004: Predictability of precipitation from continental radar images. Part III: Operational nowcasting implementation (MAPLE). *Journal of Applied Meteorology*, **43**, 231–248.

Tuttle, J. D. and G. B. Foote, 1990: Determination of the boundary layer airflow from a single doppler radar. *Journal of Atmospheric and Oceanic Technology*, **7**, 218–232.

Veneziano, D., R. L. Bras, and J. D. Niemann, 1996: Nonlinearity and self-similarity of rainfall in time and a stochastic model. *Journal of Geophysical Research*, **101**, (D21), 26,371–26,392.

Welch, G. and G. Bishop, 2001: An introduction to the Kalman filter. *Course given on Special Interest Group on Graphics and Interactive Techniques (SIGGRAPH), Los Angeles, U.S.A., 12 - 17 August 2001*.

Wilson, J. W., E. E. Ebert, T. R. Saxen, R. D. Roberts, C. K. Mueller, M. Sleigh, C. E. Pierce, and A. Seed, 2004: Sydney 2000 Forecast Demonstration Project: Convective storm nowcasting. *Weather and Forecasting*, **19**, 131–150.

Wolfson, M. M., B. E. Forman, R. G. Hallowell, and M. P. Moore, 1999: The growth and decay storm tracker. *Eighth Conf. on Aviation, Range, and Aerospace Meteorology, Dallas, TX, Amer. Meteor. Soc.*, 58–62.

**Quantitative Precipitation Forecasts
based on radar observations:
principles, algorithms and operational systems**
dr. Maarten Reyniers